

Elliptic Involution on Knot Complements

Yang (Chris) Xiu

December 7, 2015

Abstract

We show that Bordered Heegaard Floer invariant \widehat{CFD} of a knot complement in S^3 is invariant under the elliptic involution on its boundary.

1 Introduction

Heegaard Floer homology is a 3-manifold invariant defined by Peter S. Ozsváth and Zoltán Szabó in [2], which has proved to be powerful. A knot version is later defined independently by Jacob Rasmussen in [1] and by Ozsváth and Szabó in [6].

Bordered Floer homology developed by Lipshitz, Ozsváth, and Thurston in [4] is a great tool to compute Heegaard Floer homology by decomposing a 3-manifold into smaller pieces with parametrized boundaries, computing the “Bordered” invariant on each piece, and finally taking an appropriate tensor product to recombine them. Specifically, the following theorem is proved in [4].

Theorem 1. *Suppose that F is a closed oriented surface and Y_1 and Y_2 are two 3-manifolds with parametrized boundary F and $-F$, then*

$$\widehat{CF}(Y_1 \cup_F Y_2) \cong \widehat{CFA}(Y_1) \tilde{\otimes}_{\mathcal{A}(F)} \widehat{CFD}(Y_2) \cong \widehat{CFA}(Y_1) \boxtimes_{\mathcal{A}(F)} \widehat{CFD}(Y_2)$$

One natural question to ask is what happens to \widehat{CFD} modules when the boundary parametrization of a bordered manifold changes. We prove the following result:

Theorem 2. *Given a knot $K \subset S^3$, let X be the knot complement with boundary parametrization $\phi : T^2 \rightarrow \partial X$. Let $h : T^2 \rightarrow T^2$ be the elliptic involution on the torus. We have*

$$\widehat{CFD}(X, \phi) \simeq \widehat{CFD}(X, \phi \circ h).$$

One application of this result is to study 3-manifold mutations. It trivially follows that

Proposition 1. *A mutation using an elliptic involution is not detected by \widehat{HF} when either one of the two manifold with boundary is a knot complement.*

It is interesting to compare with the result in [7], where mutations using genus-2 hyperelliptic involution are studied. It is shown there that mutating by the genus-2 hyperelliptic involution can change the rank of the non-torsion summands of \widehat{HF} .

In this paper, we first introduce the necessary background in section 2, then we prove Theorem 2 in section 3, where two proofs are given. The first one in section 3.3 is simpler and more intuitive, but requires the knot to satisfy an extra mild condition. Although we are not aware of any knots that do not satisfy this condition, a general proof is given in section 3.4.

2 Background

2.1 Knot Floer Homology

We first review the setup of Knot Floer Homology, especially the aspects important to the purpose of this paper, following an overview in [4]. Suppose that a knot K is specified by a doubly-pointed Heegaard diagram $\mathcal{H} = (\Sigma, \alpha, \beta, w, z)$, where the base points are w and z . CFK^- is a \mathbb{Z} -filtered chain complex generated over $\mathbb{F}_2[U]$ by \mathfrak{S}_K , which is the usual generators of Heegaard Floer homology from diagram \mathcal{H} , with the differential

$$\partial^-(x) := \sum_{y \in \mathfrak{S}_K} \sum_{\substack{B \in \tilde{\pi}_2(x, y) \\ \text{ind}(B)=1}} \#(\mathcal{M}^B(x, y)) U^{n_w(B)} \cdot y.$$

We summarize how Maslov grading and Alexander filtration interact with the differential. If $B \in \tilde{\pi}(x, y)$, then

$$\begin{aligned} A(x) - A(y) &= n_z(B) - n_w(B) \\ A(U \cdot x) &= A(x) - 1 \\ M(x) - M(y) &= \text{ind}(B) - 2n_w(B) \\ M(U \cdot x) &= M(x) - 2 \end{aligned} \tag{1}$$

We denote $\widehat{gCFK}(\mathcal{H}, w, z)$ by C and its summand in Alexander grading r by $C(r)$. Let $\partial^i : C(r) \rightarrow C(r + i)$ be the map counting holomorphic disks ϕ with

$n_z(\phi) = -i$ and $n_w(\phi) = 0$ if $i \leq 0$, and holomorphic disks ϕ with $n_z(\phi) = 0$ and $n_w(\phi) = i$ if $i \geq 0$. Note ∂^i drops (or raises) the Alexander grading by r . Also define $\partial_w := \sum_{i \geq 0} \partial^i$ and $\partial_z := \sum_{i \leq 0} \partial^i$.

C has two filtrations, $C(\geq s) := \bigoplus_{r \geq s} C(r)$ and $C(\leq s) := \bigoplus_{r \leq s} C(r)$, preserved by ∂_w and ∂_z respectively. We primarily use $(C(\leq s), \partial_w)$, defined to be the quotient of (C, ∂_w) by subcomplex $(C(\geq s+1), \partial_w)$. Similarly, $(C(\geq s), \partial_z) := (C, \partial_z)/(C(\leq s-1), \partial_z)$.

2.2 Bordered Theory

The usage of bordered theory in this paper follows [4], primarily Chapter 11.

3 Proof of Theorem 2

The structure of this section is as follows. In section 3.1 and section 3.2, we lay the ground work for proving Theorem 2, where we argue that Proposition 2 implies Theorem 2. In section 3.3, we first prove Proposition 2 with an extra mild assumption, and then prove it in general in section 3.4.

3.1 Main idea of the proof

The proof of Theorem 2 relies on the fact that the \widehat{CFD} invariant of a knot complement can be extracted from CFK^- of the knot in a purely algorithmic fashion. We include two theorems describing this process from [4]. Specifically, Theorem 3 is the general procedure, while Theorem 4 gives us a simpler algorithm by specifying bases of CFK^- . Theorem 4 will help us arrive at a simpler proof of Theorem 2 at the expense of one extra assumption in this section. In section 3.4, we prove Theorem 2 without the assumption using Theorem 3.

We interpret the result in terms of arrows for the convenience of our later proof.

Theorem 3 (11.35, A.11 [4]). *Let $K \subset S^3$ be a knot with meridian μ and 0-framed longitude λ . Given a large enough positive integer n , $\widehat{CFD}(S^3 \setminus \text{nb}d(K))$, with framing $-n$, denoted by \widehat{CFD} for convenience, can be described by the following.*

$$\iota_0 \widehat{CFD} := \bigoplus_{s \in \mathbb{Z}} V_s^0 \quad \text{and} \quad \iota_1 \widehat{CFD} := \bigoplus_{s \in \mathbb{Z} + \frac{n+1}{2}} V_s^1,$$

where

$$V_s^0 := C(s)$$

$$V_s^1 := \begin{cases} C(\leq s + \frac{n-1}{2}) & \text{if } s \leq -\frac{n}{4} \\ \mathbb{F}_2 & \text{if } |s| < \frac{n}{4} \\ C(\geq s - \frac{n-1}{2}) & \text{if } s \geq \frac{n}{4} \end{cases}$$

The differentials are described below:

- Arrows with only idempotents:
 - within $V_s^0 = C(s)$, they are ∂^0 from the knot complex;
 - within $V_s^1 = C(\leq s + \frac{n-1}{2})$, when $s \leq -\frac{n}{4}$, they are the same as ∂_w ;
 - within $V_s^1 = C(\geq s - \frac{n-1}{2})$, when $s \geq \frac{n}{4}$, they are the same as ∂_z ;
 - within $V_s^1 = \mathbb{F}_2$, when $|s| < \frac{n}{4}$, there are none.
- Arrows with ρ_1 :
 - from $V_s^0 = C(s)$ to $V_{s+\frac{n-1}{2}}^1 = C(\geq s)$, they are the same as the inclusion of the subcomplex.
- Arrows with ρ_2 :
 - from $V_s^1 = C(\leq s + \frac{n-1}{2})$ to $V_{s+\frac{n+1}{2}}^0 = C(s + \frac{n+1}{2})$, they are the same as the composition of maps:

$$\pi \circ \partial_w : C(\leq s + \frac{n-1}{2}) \rightarrow C(s + \frac{n+1}{2}),$$
 where $\pi : C \rightarrow C(s + \frac{n+1}{2})$ is the projection.
- Arrows with ρ_3 :
 - from $V_s^0 = C(s)$ to $V_{s-\frac{n-1}{2}}^1 = C(\leq s)$, they are the same as the inclusion of the subcomplex.
- There are no arrows with ρ_{12} .
- Arrows with ρ_{23} :
 - for $s < -\frac{n}{4}$, from $V_s^1 = C(\leq s + \frac{n-1}{2})$ to $V_{s+1}^1 = C(\leq s + \frac{n+1}{2})$, they are the same as the inclusion of the subcomplex;
 - for $s \leq -\frac{n}{4} < s + 1$, from $V_s^1 = (C, \partial_w)$ to $V_{s+1}^1 = \mathbb{F}_2$, they are the same as a chain map inducing an isomorphism in homology;

- for $|s| < \frac{n-2}{4}$, from $V_s^1 = \mathbb{F}_2$ to $V_{s+1}^1 = \mathbb{F}_2$, it is the unique isomorphism;
- for $s < \frac{n}{4} \leq s+1$, from $V_s^1 = \mathbb{F}_2$ to $V_{s+1}^1 = (C, \partial_z)$, they are the same as a chain map inducing an isomorphism in homology;
- for $s > \frac{n}{4}$, from $V_s^1 = C(\geq s - \frac{n-1}{2})$ to $V_{s+1}^1 = C(\geq s - \frac{n+1}{2})$, they are the same as the projection map.

• Arrows with ρ_{123} :

- from $V_s^0 = C(s)$ to $V_{s+\frac{n+1}{2}}^1 =$, they are the same as the composition of maps:

$$i \circ \partial_w^1 : C(s) \rightarrow (C(\geq s+1), \partial_z),$$

where $i : C(s+1) \rightarrow (C(\geq s+1), \partial_z)$ is the inclusion.

The following is the same procedure described in terms of bases of $CFK^-(K)$, which turns out to be more intuitive.

Theorem 4 (11.27, A.11 [4]). *Given a knot $K \subset S^3$, let X be the knot complement with boundary parametrization $\phi : T^2 \rightarrow \partial X$ corresponding to an integral framing n . Let $CFK^-(K)$ be a reduced model for the knot Floer complex of K admitting a basis $\{\xi_i\}$ which is simultaneously vertically and horizontally simplified. Suppose ξ_v (respectively ξ_h) is the generator of $CFK^-(K)$ which has no in-coming or out-going vertical (respectively horizontal) arrows. Apply the following procedure to get $\widehat{CFD}(X, \phi)$:*

$\iota_0 \widehat{CFD}(X, \phi)$ is identified with $CFK^-(K)$ as an \mathbb{F}_2 -module. Denote the corresponding generators of $\iota_0 \widehat{CFD}(X, \phi)$ by ξ'_1, ξ'_2, \dots .

For each vertical arrow of length ℓ from ξ_i to ξ_{i+1} , we associate a string of basis elements $\kappa_1^i, \kappa_2^i, \dots, \kappa_\ell^i$ for $\iota_1 \widehat{CFD}(X, \phi)$ and differentials among them:

$$\xi'_i \xrightarrow{\rho_1} \kappa_1^i \xleftarrow{\rho_{23}} \dots \xleftarrow{\rho_{23}} \kappa_k^i \xleftarrow{\rho_{23}} \kappa_{k+1}^i \xleftarrow{\rho_{23}} \dots \xleftarrow{\rho_{23}} \kappa_\ell^i \xleftarrow{\rho_{123}} \xi'_{i+1}$$

For each horizontal arrow of length ℓ from ξ_j to ξ_{j+1} , we associate a string of basis elements $\lambda_1^j, \lambda_2^j, \dots, \lambda_\ell^j$ for $\iota_1 \widehat{CFD}(X, \phi)$ and differentials among them:

$$\xi'_j \xrightarrow{\rho_3} \lambda_1^j \xrightarrow{\rho_{23}} \dots \xrightarrow{\rho_{23}} \lambda_k^j \xrightarrow{\rho_{23}} \lambda_{k+1}^j \xrightarrow{\rho_{23}} \dots \xrightarrow{\rho_{23}} \lambda_\ell^j \xrightarrow{\rho_2} \xi'_{j+1}$$

We include one more string of generators and differentials called the unstable chain, depending on framing n . When $n < 2\tau(K)$, it takes form:

$$\xi'_v \xrightarrow{\rho_1} \mu_1 \xleftarrow{\rho_{23}} \dots \xleftarrow{\rho_{23}} \mu_k \xleftarrow{\rho_{23}} \mu_{k+1} \xleftarrow{\rho_{23}} \dots \xleftarrow{\rho_{23}} \mu_m \xleftarrow{\rho_3} \xi'_h,$$

where $m = 2\tau(K) - n$. When $n = 2\tau(K)$, it takes form:

$$\xi'_v \xrightarrow{\rho_{12}} \xi'_h.$$

When $n > 2\tau(K)$, it takes form,

$$\xi'_v \xrightarrow{\rho_{123}} \mu_1 \xrightarrow{\rho_{23}} \cdots \xrightarrow{\rho_{23}} \mu_k \xrightarrow{\rho_{23}} \mu_{k+1} \xrightarrow{\rho_{23}} \cdots \xrightarrow{\rho_{23}} \mu_m \xrightarrow{\rho_2} \xi'_h,$$

where $m = n - 2\tau(K)$.

We then layout some basic definitions for our proof.

Definition 1. Denote the type D module resulted from applying the procedures in Theorem 3 or Theorem 4 to a complex C by $KtD(C)$, standing for CFK^- to \widehat{CFD} .

Definition 2. Given a model C for CFK^- of a knot $K \subset S^3$ endowed with Alexander filtration A and Maslov grading M , we defined the flipped complex C^{flip} resulted from switching horizontal and vertical arrows of C as follows:

We take $C^{flip} \cong C$ as a $\mathbb{F}_2[U]$ -module, i.e. there is an isomorphism $C \rightarrow C^{flip}$ taking a generator x of C to a generator x^{flip} of C^{flip} .

Define a Maslov grading on C^{flip} by $M(x^{flip}) = M(x) - 2A(x)$

Define an Alexander filtration on C^{flip} by $A(x^{flip}) = -A(x)$.

For each arrow in C of the form $x \rightarrow U^r y$ with $A(x) - A(y) = s$, we assign an arrow in C^{flip} of the form $x^{flip} \rightarrow U^{r+s} y^{flip}$.

Lemma 1. C^{flip} constructed in Definition 2 is indeed a chain complex and all horizontal and vertical arrows are switched. Furthermore, if C is computed directly from a Heegaard diagram $(\Sigma, \alpha, \beta, w, z)$, then C^{flip} is isomorphic to the knot Floer complex C' computed from $(\Sigma, \alpha, \beta, z, w)$ up to overall Maslov grading and Alexander filtration shifts.

Proof. We begin by observing that arrow $x \rightarrow U^r y$ with $A(x) - A(y) = s$ drops Alexander filtration by $A(x) - A(U^r y) = r + s$ and U -filtration by r , by eq. (1). The new arrow in C^{flip} of form $x^{flip} \rightarrow U^{r+s} y^{flip}$ drops Alexander filtration by $A(x^{flip}) - A(U^{r+s} y^{flip}) = -(A(x) - A(y)) + r + s = r$, and the U -filtration by $r + s$. Graphically, the arrow in C represented by a vector $(-r - s, -r)$ is now assigned an

arrow in C^{flip} represented by $(-r, -r - s)$. For the Maslov grading, the new arrow drops it by

$$\begin{aligned} M(x^{flip}) - M(U^{r+s}y^{flip}) &= M(x^{flip}) - M(y^{flip}) + 2r + 2s \\ &= (M(x) - M(y)) - 2(A(x) - A(y)) + 2r + 2s \\ &= M(x) - M(y) + 2r = M(x) - M(U^r y) = 1, \end{aligned}$$

which means the Maslov grading on C^{flip} is respected by the differential. $\partial^2 = 0$ is obvious as it is equivalent to there being even number of two-step paths from any given generator to any other generator in C^{flip} . This is true for C and graphically arrows in C^{flip} are just those in C flipped across the diagonal.

Now suppose C is computed directly from a Heegaard diagram $(\Sigma, \alpha, \beta, w, z)$. We denote the knot Floer complex computed from $(\Sigma, \alpha, \beta, z, w)$ by C' . Generators of C' , which we denote by x', y' , etc., are in one-to-one correspondence with generators x, y , etc. of C , hence matching those of C^{flip} .

For each arrow in C of form $x \rightarrow U^r y$ with $A(x) - A(y) = s$, represented by $B \in \tilde{\pi}_2(x, y)$, it follows from eq. (1) that $s = A(x) - A(y) = n_z(B) - n_w(B)$ and $M(x) - M(y) = \text{ind}(B) - 2n_w(B)$. As C' is computed from the same Heegaard diagram except with interchanged basepoints, the same holomorphic disk also contributes in C' , denoted by $B' \in \tilde{\pi}_2(x', y')$ satisfying $n_w(B') = n_z(B)$ and $n_z(B') = n_w(B)$. Now we have

$$\begin{aligned} A(x') - A(y') &= n_z(B') - n_w(B') = n_w(B) - n_z(B) = -(A(x) - A(y)) \\ M(x') - M(y') &= \text{ind}(B') - 2n_w(B') = \text{ind}(B) - 2n_z(B) \\ &= \text{ind}(B) - 2n_w(B) - 2(n_z(B) - n_w(B)) \\ &= M(x) - M(y) - 2(A(x) - A(y)) \end{aligned} \tag{2}$$

Note $n_w(B') = n_z(B) = n_w(B) + s = r + s$, so there exists an arrow in C' of form $x' \rightarrow U^{r+s}y'$ with $A(x') - A(y') = -s$, which agrees with our construction of C^{flip} .

It is known that the values of $A(x') - A(y')$ and $M(x') - M(y')$ for all x', y' and $B' \in \tilde{\pi}_2(x', y')$ completely determine the Maslov grading and Alexander filtration of C' up to overall translations. So the fact that our construction of A and M on C^{flip} satisfies eq. (2) let us conclude that C^{flip} and C' are indeed isomorphic. \square

By Theorem 11 in [5], $\widehat{CFD}(X, \phi \circ h) = \widehat{CFDA}(h) \boxtimes \widehat{CFD}(X, \phi)$. In order to prove Theorem 2, we need to compute $\widehat{CFDA}(h) \boxtimes \widehat{CFD}(X, \phi)$. To do this, we prove the following proposition, which implies Theorem 2 immediately:

Proposition 2. *Given a knot $K \subset S^3$, let X be the knot complement with boundary parametrization $\phi : T^2 \rightarrow \partial X$ corresponding to a integral framing $n \leq 2\tau(K) - 3$. Let C be a reduced and horizontally simplified model for the knot Floer complex $CFK^-(K)$. Then $\widehat{CFDA}(h) \boxtimes \widehat{CFD}(X, \phi)$ is isomorphic to the type D module $KtD(C^{flip})$ resulted from applying the procedure in Theorem 4 to C^{flip} , i.e.*

$$\widehat{CFDA}(h) \boxtimes \widehat{CFD}(X, \phi) \simeq KtD(C^{flip}).$$

Proposition 2 implies Theorem 2 as follows.

Proof of Theorem 2 assuming Proposition 2. We fix a doubly pointed Heegaard diagram $(\Sigma, \alpha, \beta, w, z)$ for knot $K \subset S^3$ and denote by $CFK^-(K)$ the knot Floer complex computed from the diagram. $(\Sigma, \alpha, \beta, z, w)$ is a doubly pointed Heegaard diagram for knot $-K \subset S^3$. By lemma 1, switching basepoints has exactly the same effect as switching the horizontal and vertical arrows, i.e. $CFK^-(-K) = CFK^-(K)^{flip}$. It is known that $CFK^-(K) \simeq CFK^-(-K)$ from [2], so $CFK^-(K) \simeq CFK^-(K)^{flip}$. Next, we find a reduced and horizontally simplified model C of $CFK^-(K)$. The process of reducing and horizontally simplifying $CFK^-(K)$ can be flipped to reduce and vertically simplify $CFK^-(K)^{flip}$ to C^{flip} . As a result, $CFK^-(K) \simeq CFK^-(K)^{flip} \simeq C^{flip}$, which means C^{flip} is another model for the knot Floer complex $CFK^-(K)$ of knot K , so Theorem 4 implies that the type D module $KtD(C^{flip})$ that results from applying the procedure (with framing n) to C^{flip} is homotopy equivalent to $\widehat{CFD}(X, \phi)$, i.e. $KtD(C^{flip}) \simeq \widehat{CFD}(X, \phi)$. Hence for this small enough framing n , Proposition 2 implies Theorem 2. For a general framing, we obtain $\widehat{CFD}(X, \phi')$ for the desired framing by tensoring $\widehat{CFD}(X, \phi)$ with $\widehat{CFDA}(\tau_\mu)$ repeatedly. Theorem 2 is now proved by the fact $\widehat{CFDA}(h) \boxtimes \widehat{CFDA}(\tau_\mu) \cong \widehat{CFDA}(\tau_\mu) \boxtimes \widehat{CFDA}(h)$, as $h \circ \tau_\mu = \tau_\mu \circ h$ as topological maps.

□

Now all there is left to do is to prove Proposition 2.

3.2 Type DA Module H for the elliptic involution

The elliptic involution on a torus can be decomposed into $(\tau_\mu \circ \tau_\lambda)^3$, where τ_μ and τ_λ are Dehn twists along a meridian and a longitude, respectively [3]. $\widehat{CFDA}(\tau_\mu)$ is generated by p, q, r and its non-trivial algebra actions are given as follows [4]:

$$\begin{aligned}
m_{0,1,1}(p, \rho_1) &= \rho_1 \otimes q & m_{0,1,1}(p, \rho_{12}) &= \rho_{123} \otimes r \\
m_{0,1,1}(p, \rho_{123}) &= \rho_{123} \otimes q & m_{0,1,2}(p, \rho_3, \rho_2) &= \rho_3 \otimes r \\
m_{0,1,2}(p, \rho_3, \rho_{23}) &= \rho_3 \otimes q & m_{0,1,1}(q, \rho_2) &= \rho_{23} \otimes r \\
m_{0,1,1}(q, \rho_{23}) &= \rho_{23} \otimes q & m_{0,1,0}(r) &= \rho_2 \otimes p \\
m_{0,1,1}(r, \rho_3) &= q & &
\end{aligned}$$

$\widehat{CFDA}(\tau_\lambda)$ is generated by p, q, s and its non-trivial algebra actions are given as follows [4]:

$$\begin{aligned}
m_{0,1,2}(q, \rho_2, \rho_1) &= \rho_2 \otimes s & m_{0,1,2}(q, \rho_2, \rho_{12}) &= \rho_2 \otimes p \\
m_{0,1,2}(q, \rho_2, \rho_{123}) &= \rho_{23} \otimes q & m_{0,1,1}(p, \rho_1, \rho_2) &= \rho_{12} \otimes s \\
m_{0,1,1}(p, \rho_{12}) &= \rho_{12} \otimes p & m_{0,1,1}(p, \rho_{123}) &= \rho_{123} \otimes q \\
m_{0,1,1}(p, \rho_3) &= \rho_3 \otimes q & m_{0,1,0}(s) &= \rho_1 \otimes q \\
m_{0,1,1}(s, \rho_2) &= p & m_{0,1,1}(s, \rho_{23}) &= \rho_3 \otimes q
\end{aligned}$$

By Theorem 12 in [5], $H := \widehat{CFDA}(h)$ can be computed as $\widehat{CFDA}(\tau_\mu) \boxtimes \widehat{CFDA}(\tau_\lambda) \boxtimes \widehat{CFDA}(\tau_\mu) \boxtimes \widehat{CFDA}(\tau_\lambda) \boxtimes \widehat{CFDA}(\tau_\mu) \boxtimes \widehat{CFDA}(\tau_\lambda)$.

We omit the computation of the tensor product, but instead describe the type DA bimodule H that results from canceling the following arrows in the following order:

$$\begin{aligned}
p \otimes p \otimes p \otimes s \otimes r \otimes p &\rightarrow p \otimes p \otimes p \otimes p \otimes p \otimes p, \\
p \otimes p \otimes p \otimes s \otimes r \otimes s &\rightarrow p \otimes p \otimes p \otimes p \otimes p \otimes s, \\
p \otimes s \otimes r \otimes s \otimes q \otimes q &\rightarrow p \otimes p \otimes p \otimes s \otimes q \otimes q, \\
p \otimes s \otimes r \otimes s \otimes r \otimes p &\rightarrow p \otimes s \otimes r \otimes p \otimes p \otimes p, \\
p \otimes s \otimes r \otimes s \otimes r \otimes s &\rightarrow p \otimes s \otimes r \otimes p \otimes p \otimes s, \\
q \otimes q \otimes r \otimes s \otimes r \otimes p &\rightarrow q \otimes q \otimes r \otimes p \otimes p \otimes p, \\
q \otimes q \otimes r \otimes s \otimes r \otimes s &\rightarrow q \otimes q \otimes r \otimes p \otimes p \otimes s, \\
r \otimes p \otimes p \otimes s \otimes r \otimes p &\rightarrow r \otimes p \otimes p \otimes p \otimes p \otimes p, \\
r \otimes p \otimes p \otimes s \otimes r \otimes s &\rightarrow r \otimes p \otimes p \otimes p \otimes p \otimes s, \\
r \otimes s \otimes q \otimes q \otimes r \otimes s &\rightarrow q \otimes q \otimes r \otimes s \otimes q \otimes q, \\
r \otimes s \otimes r \otimes s \otimes q \otimes q &\rightarrow r \otimes p \otimes p \otimes s \otimes q \otimes q,
\end{aligned}$$

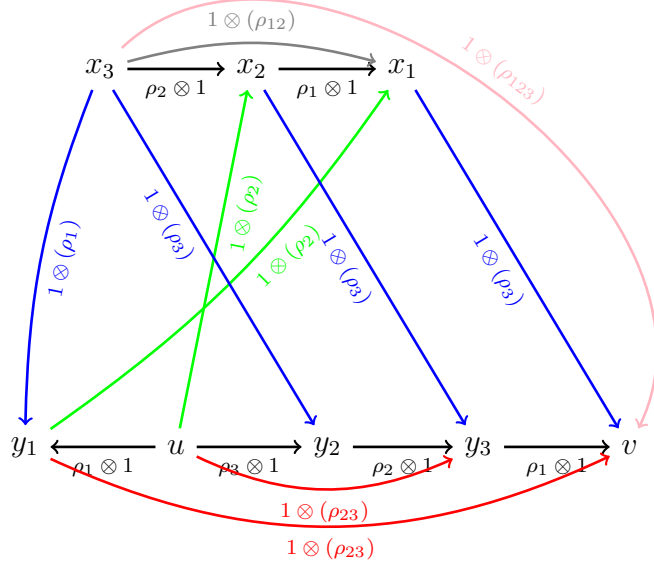


Figure 1: Arrows are color coded according to their A^∞ actions.

$$\begin{aligned}
 r \otimes s \otimes r \otimes s \otimes r \otimes p &\rightarrow r \otimes s \otimes r \otimes p \otimes p \otimes p, \\
 r \otimes s \otimes r \otimes s \otimes r \otimes s &\rightarrow r \otimes s \otimes r \otimes p \otimes p \otimes s.
 \end{aligned}$$

For simplicity, we rename the remaining generators $r \otimes s \otimes q \otimes q \otimes r \otimes p, q \otimes q \otimes q \otimes q \otimes r \otimes p, p \otimes s \otimes q \otimes q \otimes r \otimes p, q \otimes q \otimes q \otimes q \otimes q \otimes q, p \otimes s \otimes q \otimes q \otimes r \otimes s, p \otimes s \otimes q \otimes q \otimes q \otimes q, r \otimes s \otimes q \otimes q \otimes q \otimes q, q \otimes q \otimes q \otimes q \otimes r \otimes s$ with $x_3, x_1, x_2, v, u, y_3, y_2, y_1$, respectively. Generators x_1, x_2, x_3 have idempotent ι_0 and generators u, v, y_1, y_2, y_3 have idempotent ι_1 . Now H can be described as in fig. 1.

Throughout this paper, we adapt the following color code for arrows: We use color blue, green, blue, red, and pink for D -side arrows with $\rho_1, \rho_2, \rho_3, \rho_{23}$, and ρ_{123} respectively, and for A -side arrows with A^∞ action of $\rho_1, \rho_2, \rho_3, \rho_{23}$, and ρ_{123} respectively. Finally, when tensoring arrows with the same color from both sides, we generally keep the color for the resulted arrow in the tensor product.

3.3 Proof of the Case of simplified CFK^-

We first prove Proposition 2 with an extra assumption. See section 3.4 for the general proof. In this section, we assume that we have a model C of $CFK^-(K)$ which is

simultaneously horizontally and vertically simplified. We remark that even though there exist examples of filtered chain complexes that can not be simultaneously horizontally and vertically simplified, we are not aware of any examples that can be realized as CFK^- of a knot.

Recall our notation, $H = \widehat{CFDA}(h)$, where h is the elliptic involution and $KtD(C)$ (respectively, $KtD(C^{flip})$) is the type D module resulted from applying the procedure in Theorem 4 to C (respectively, C^{flip}).

3.3.1 A string of ρ_{23} 's

According to Theorem 4, the middle part of each chain of arrows in $KtD(C)$ is a (possibly empty) string of ρ_{23} 's. We first investigate how H acts on a string of ρ_{23} 's,

$$\dots \xrightarrow{\rho_{23}} * \xrightarrow{\rho_{23}} * \xrightarrow{\rho_{23}} * \xrightarrow{\rho_{23}} * \dots$$

The result of the tensor product is shown in fig. 2b, and after we cancel all the red arrows, the result is a string of ρ_{23} 's going the opposite direction, shown in fig. 2c.

We observe that for each vertical arrow $\xi_i \rightarrow \xi_j$, the corresponding chain in $KtD(C)$ has a string of ρ_{23} 's in the *opposite* direction as the original arrow, where by *opposite* we mean pointing toward ξ'_i and away from ξ'_j . For each horizontal arrow $\xi_i \rightarrow \xi_j$ in C^{flip} , the corresponding chain in $KtD(C^{flip})$ has a string of ρ_{23} 's in the *same* direction as the original arrow, where by *same* we mean pointing away from ξ'_i and toward from ξ'_j . The box tensor product of H with a string of ρ_{23} 's gives exactly the correspondence between the “middle” parts of the two corresponding chains.

Now we investigate how the joints between these strings of ρ_{23} 's are also “flipped” by tensoring with H .

Since C is both horizontally and vertically simplified, at any generator $\xi_i \neq \xi_v$ or ξ_h , we have the following four kinds of joints in fig. 3.

For each kind of joint at ξ_i , we argue the corresponding joint at ξ'_i in $KtD(C)$ can be identified with a joint in $KtD(C^{flip})$ by tensoring with H . Our way of doing this is simply through cancellation in $H \boxtimes KtD(C)$ and match the result to the corresponding part of $KtD(C^{flip})$. Then what is left to show $H \boxtimes KtD(C) = KtD(C^{flip})$ is how these cancellation at different parts of $H \boxtimes KtD(C)$ agree with each other.

We organize as follows the proof of that the “local” cancellations agree: if an arrow at ξ_i in C has length more than 1, then the chain of arrows at ξ'_i in $KtD(C)$ is connected to a string of ρ_{23} 's. We observe how the cancellation at this joint in $H \boxtimes KtD(C)$ agree with the cancellation we perform for a string of ρ_{23} 's, so the chain of ρ_{23} 's along with the end point ξ'_i is matched to a flipped chain in $KtD(C^{flip})$. If an

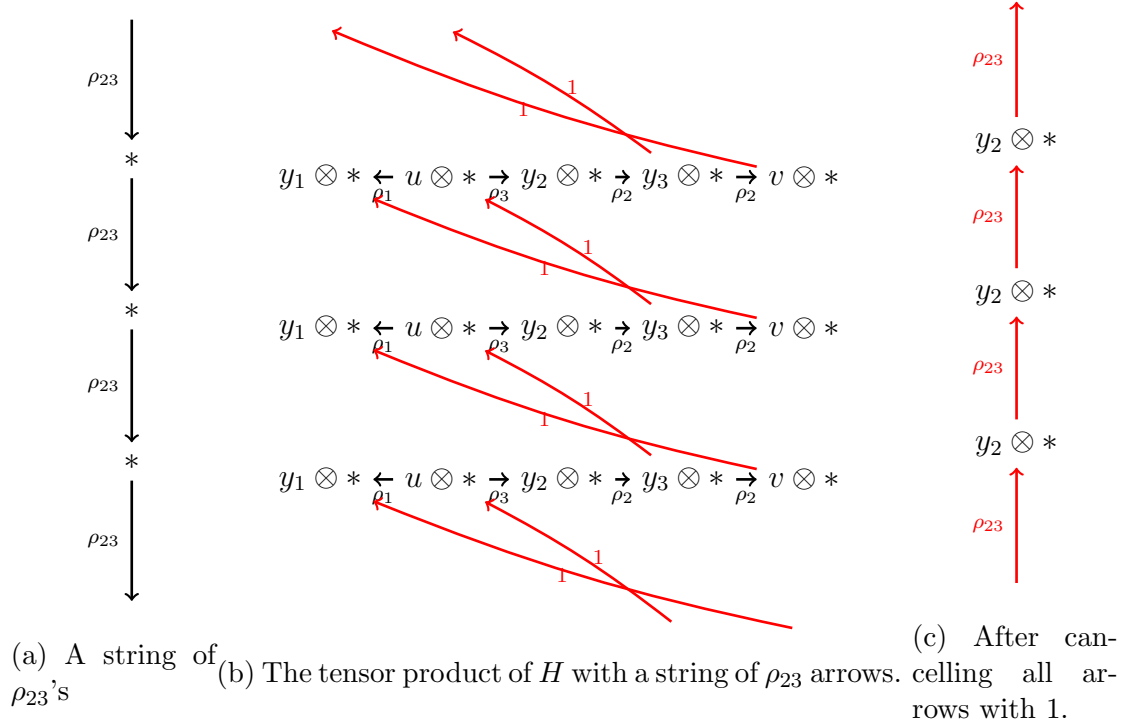


Figure 2: H tensoring with a string of ρ_{23} 's.

arrow at ξ_i in C has length exactly 1, ξ'_i in $KtD(C)$ is connected to another generator ξ'_j through a short chain of two arrows. After we discuss the cancellation *at both* of these joint, we show it agrees and gives the desired result when the two joint are put together.

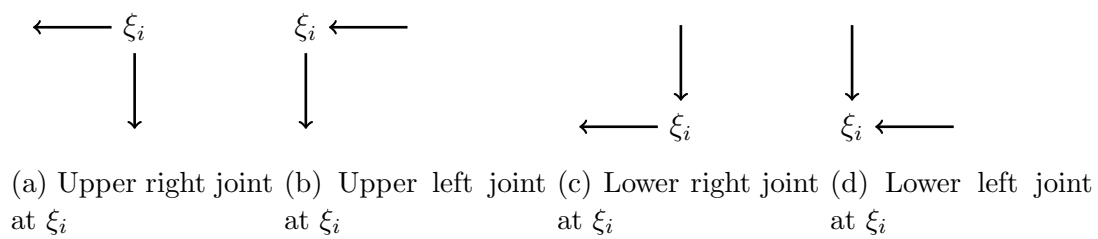


Figure 3: Four kinds of joints at $\xi_i \neq \xi_v$ or ξ_h

3.3.2 Upper right joint

For a generator ξ_i with the upper right joint in fig. 3, it appears in $KtD(C)$ as fig. 4a. For either of the two arrows not immediately connecting to ξ'_i , we have two possibilities, corresponding to original arrows in C having length 1 or having length more than 1.

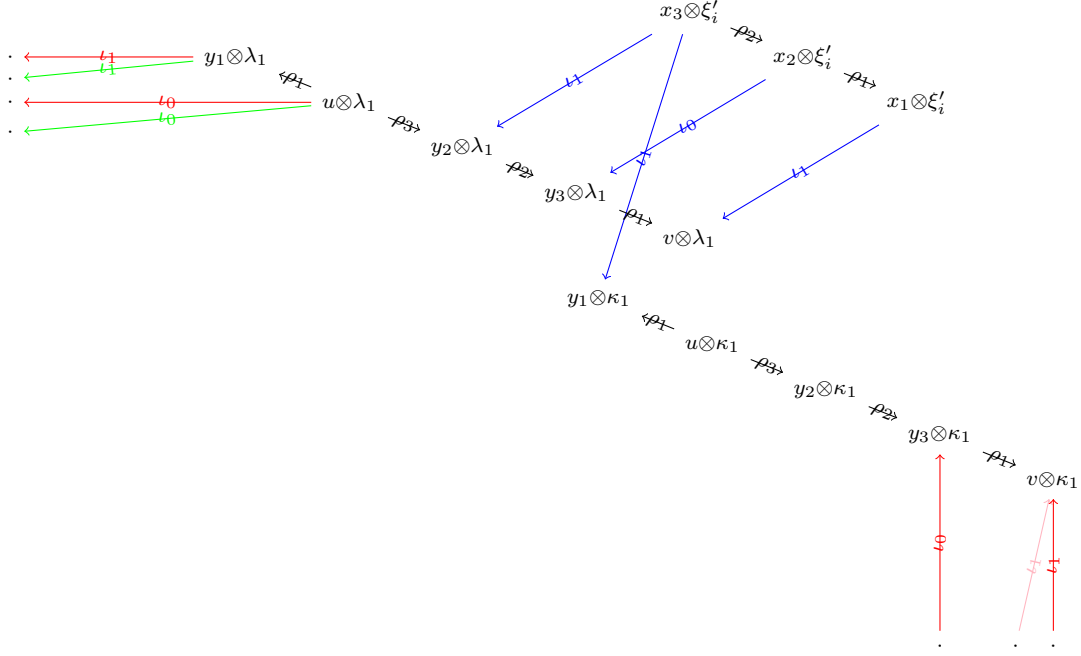
To be concise, the corresponding part of the box tensor product $H \boxtimes KtD(C)$ for all four cases are shown in fig. 4b, where all four cases share the same generators and arrows in blue. On the left side, the two red arrows (two green arrows, respectively) come from cases where the arrow out of λ_1 is ρ_{23} (ρ_2 , respectively). Similarly, on the bottom right, the two red arrows (one pink arrow, respectively) come from cases where the arrow into κ_1 is ρ_{23} (ρ_{123} , respectively).

Now cancel the three blue arrows that are pointing leftward and rearrange generators to arrive at fig. 4c. Note the joint at $u \otimes \kappa_1$ in $H \boxtimes KtD(C)$, which is boxed in fig. 4c, can now be identified with the corresponding part of $KtD(C^{flip})$.

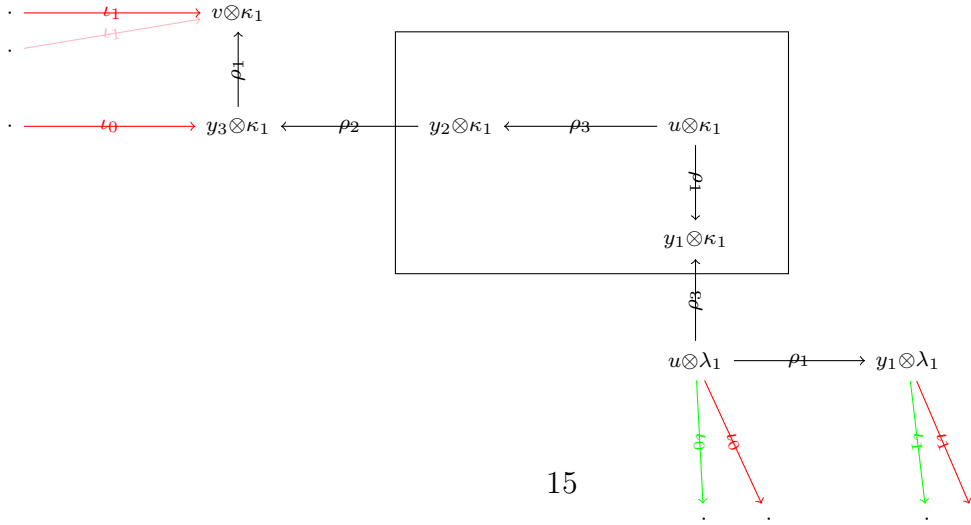
If either of the two possibilities is ρ_{23} , we can continue to cancel the set of two red arrows in fig. 4c in the same way we canceled arrows in the case of a string of ρ_{23} 's, then arrive at fig. 5a. In these cases, cancellation done here agree with those in the case of tensoring with a string of ρ_{23} 's, so chains containing ρ_{23} 's at $u \otimes \kappa_1$ in $H \boxtimes KtD(C)$ can be identified with chains in $KtD(C^{flip})$, compare with fig. 4a. Arrows in cases where either arrow at ξ_i have length 1 will be brought into shape after we deal with the joints ξ_i is connected to.

$$\begin{array}{c}
\begin{array}{ccccc}
& \xleftarrow{\frac{\rho_{23}}{\rho_2}} & \lambda_1 & \xleftarrow{\rho_3} & \xi'_i \\
& & & \downarrow \rho_1 & \\
& & & \kappa_1 & \\
& & \uparrow \rho_{123} & & \\
& & \rho_{23} & &
\end{array}
\end{array}$$

(a) Upper right joint at ξ_i

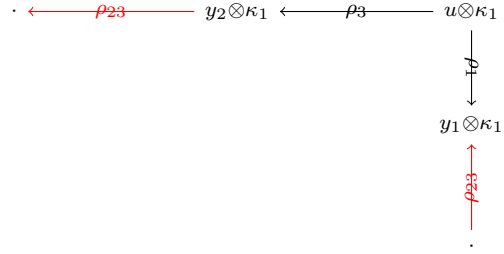


(b) H box tensor product with the joint.



(c) After canceling the three blue arrows pointing left

Figure 4: Upper right joint



(a) Cases where either arrow at ξ'_i have length more than 1.

Figure 5: Upper right joint

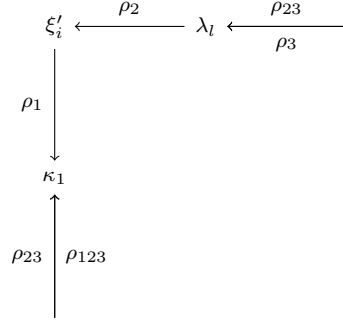
3.3.3 Upper left joint

For a generator ξ_i with the upper left joint in fig. 3, it appears in $KtD(C)$ as fig. 6a. For either of the two arrows not immediately connecting to ξ'_i , we have two possibilities, corresponding to original arrows in C having length 1 or having length more than 1. To be concise, the corresponding part of the box tensor product $H \boxtimes KtD(C)$ for all four cases are shown in fig. 6b, where all four cases share the same generators and arrows in the middle. On the right side, the two red arrows (three blue arrows, respectively) come from cases where in fig. 6a the arrow going into λ_ℓ has a ρ_{23} (ρ_3 , respectively). Similarly, on bottom left, the two red arrows (one pink arrow, respectively) come from cases where the arrow going into κ_1 has a ρ_{23} (ρ_{123} , respectively).

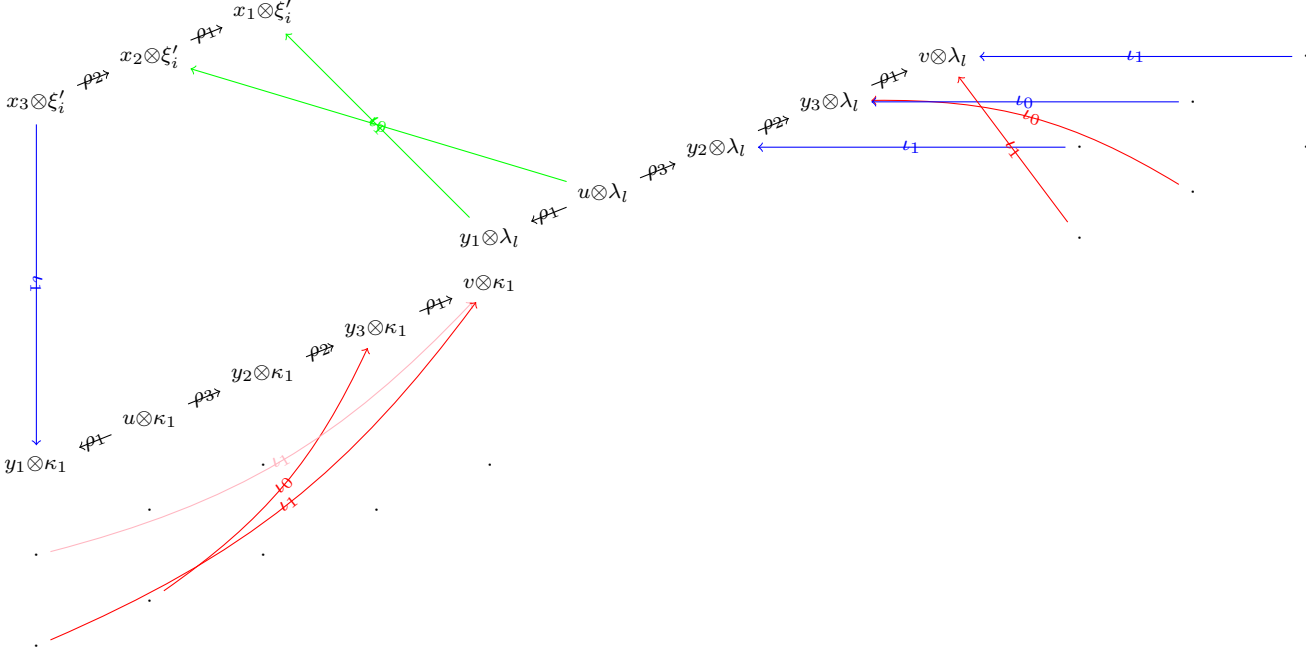
Then we cancel the blue arrow and the two green arrows in the middle and arrive at fig. 7a. Note the joint at $u \otimes \kappa_1$, which is boxed in fig. 7a, can now be matched exactly to the corresponding part of $KtD(C^{flip})$, which would look like fig. 9a.

If either of the two possibilities is ρ_{23} , we observe that cancellation of either set of two red arrows in fig. 7a agree with the cancellations for a string of ρ_{23} 's in section 3.3.1, which shows chains containing ρ_{23} 's at $u \otimes \kappa_1$ in $H \boxtimes KtD(C)$ (fig. 7b) exactly match corresponding chains in $KtD(C^{flip})$, again see fig. 9a.

If the horizontal arrow at λ_ℓ has a ρ_3 coming in, see fig. 6a, meaning original arrow out of ξ_i has length 1, the ρ_3 must come from another ξ'_j . ξ'_j belongs to either a upper right joint or a lower right joint. We defer the latter case to the lower right joint section, section 3.3.4. In the former case, we combine the tensor product here and the tensor product fig. 4b in section 3.3.2. Now $\lambda_\ell = \lambda_1$ and the green arrows in fig. 6b and fig. 4b are identified, so are the three horizontal blue arrows in fig. 6b and fig. 4b. Reviewing the cancellation in this section and the upper right joint section, we find they combine together without conflicting and result in fig. 7c, which is what the corresponding part in $KtD(C^{flip})$ look like.

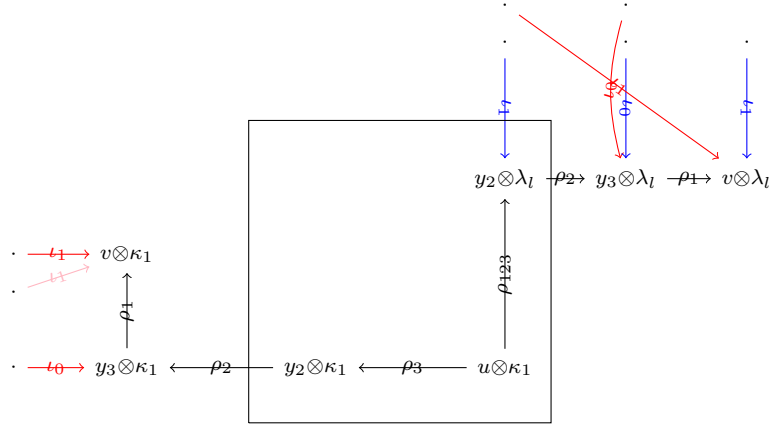


(a) Upper left joint at ξ'_i

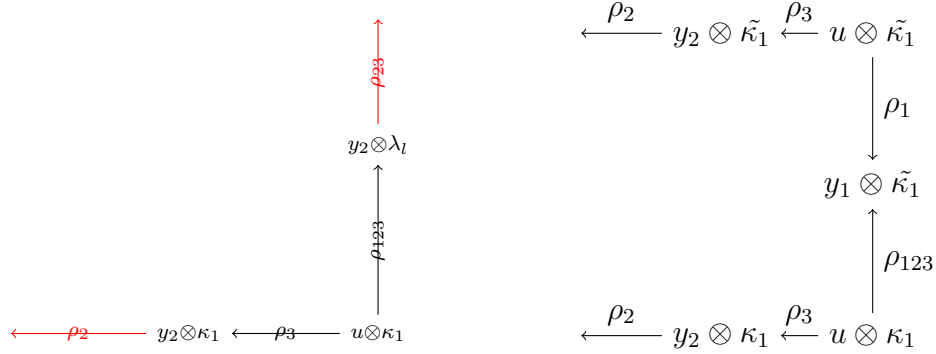


(b) Tensor product with H .

Figure 6: Upper left joint.



(a) After cancellation.



(b) Cases where either arrow at ξ'_i have length more than 1 (c) Upper left joint connected to a upper right joint.

Figure 7: Upper left joint.

3.3.4 Lower right joint

For a generator ξ_i with the lower right joint in fig. 3, it appears in $KtD(C)$ as fig. 9a. Again, for either of the two arrows not immediately connecting to ξ'_i , we have two possibilities, corresponding to original arrows in C having length 1 or having length more than 1, and the corresponding part of the box tensor product $H \boxtimes KtD(C)$ for all four cases are shown in fig. 9b, where all four cases share the same generators and arrows in the middle. On the top right, the two red arrows (one blue arrow, respectively) come from cases where in fig. 9a the arrow going out of κ_ℓ (into κ_ℓ , respectively) has a ρ_{23} (ρ_1 , respectively). Similarly, on the left side, the two red arrows (two green arrows, respectively) come from cases where the arrow going into λ_1 has a ρ_{23} (ρ_2 , respectively).

Then we cancel the three blue arrows and the pink arrow in the middle and arrive at fig. 10a. Note the joint at $y_3 \otimes \kappa_\ell$, which is boxed in fig. 10a, can now be identified with the corresponding part of $KtD(C^{flip})$, which would look like the joint in fig. 6a.

If either of the two possibilities in fig. 9a is ρ_{23} , as above, we observe that cancellation of either set of two red arrows in fig. 10a agree with the cancellations we performed for a string of ρ_{23} 's in section 3.3.1. This shows chains containing ρ_{23} 's at $y_3 \otimes \kappa_\ell$ in $H \boxtimes KtD(C)$ (fig. 10b) exactly match corresponding chains in $KtD(C^{flip})$, again see fig. 6a.

Now we deal with the possibilities other than ρ_{23} in fig. 9a. Suppose arrows at ξ_i takes form as in fig. 8.

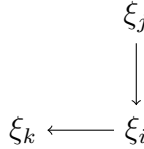


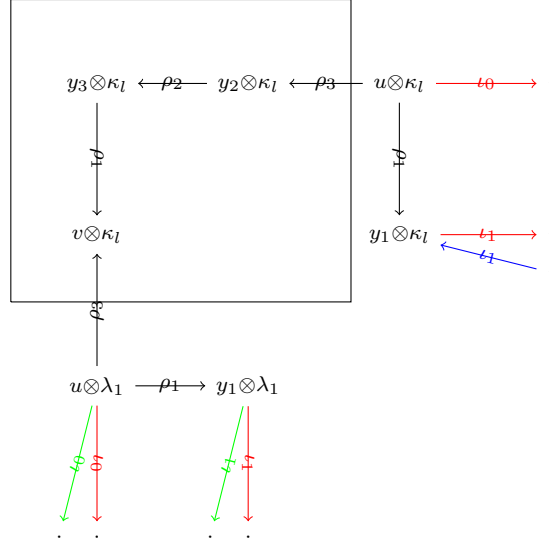
Figure 8: Lower right joint at ξ_i

If the vertical arrow $\xi_j \rightarrow \xi_i$, has length 1 in C , the joint at ξ_j could be either a upper right joint or a upper left joint. We argue that the latter case can not happen. If it did happen, denote the generator connecting to ξ_j through a horizontal arrow by ξ_r , then $\partial^2 \xi_r$ has a term $U\xi_i$. Because the C is simultaneously horizontally and vertically simplified, there can not be any arrow going into ξ_i besides $\xi_j \rightarrow \xi_i$, leaving $\partial^2 \xi_r$ nonzero.

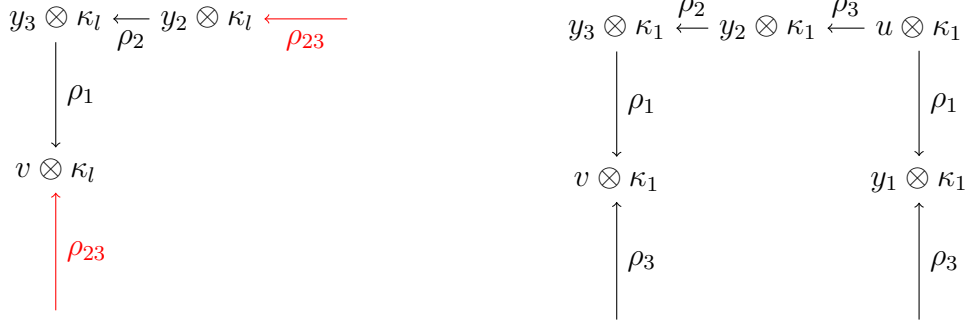
For the case where ξ_j belongs to a upper right joint, we combine the corresponding parts of $H \boxtimes KtD(C)$ in fig. 4b and fig. 9b. Now generators has κ_ℓ are identified those with κ_1 . The downward point blue arrow in fig. 4b is identified with the blue

arrow on top of fig. 9b, so are the pink arrow in each of the figures. The cancellation we performed for each type of joints can be both applied and result in fig. 10c. It can be identified with the corresponding part in $KtD(C^{flip})$.

If the horizontal arrow $\xi_i \rightarrow \xi_k$ has length 1 in C , the joint at ξ_k could be either a upper left joint or a lower left joint. We postpone the latter case to the lower left joint section, section 3.3.5. For the former case, we argue that it could not happen. $\partial^2 \xi_j$ has term $U\xi_k$, but there can not be any arrow going into ξ_k besides $\xi_i \rightarrow \xi_k$, leaving $\partial^2 \xi_j$ nonzero.



(a) After cancellation.



(b) Cases where either arrow at ξ_i^l have length more than 1 (c) A lower right joint connected to a upper right joint

Figure 10: Lower right joint

We include a summary of all eight possible ways two joints could overlap, see fig. 11.

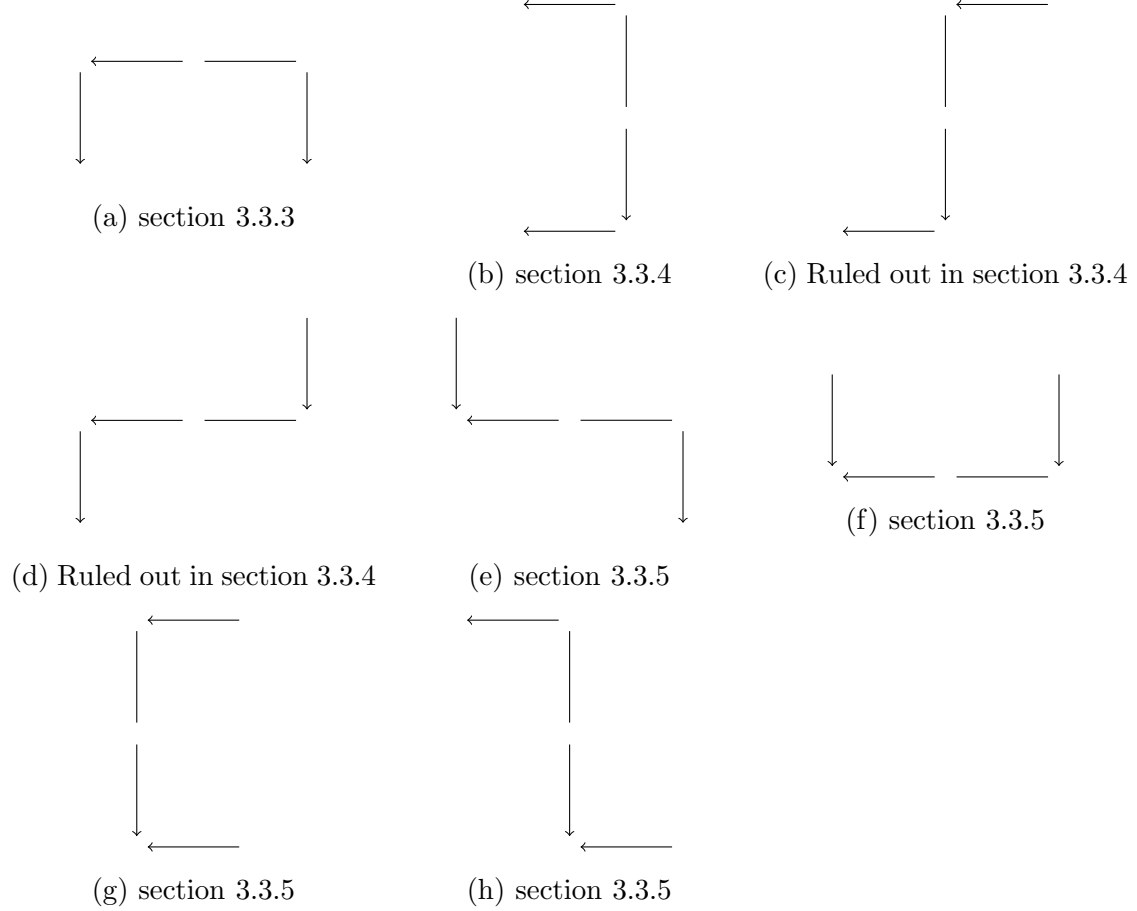


Figure 11: A summary of eight possible overlapping joints

3.3.5 Lower left joint

For a generator ξ_i with the lower left joint in fig. 3, it appears in $KtD(C)$ as fig. 12a. Again, for either of the two arrows not immediately connecting to ξ'_i , we have two possibilities, corresponding to original arrows in C having length 1 or having length more than 1, and the corresponding part of the box tensor product $H \boxtimes KtD(C)$ for all four cases are shown in fig. 12b, where all four cases share the same generators and arrows in the middle. On the top, the two red arrows (one blue arrow, respectively)

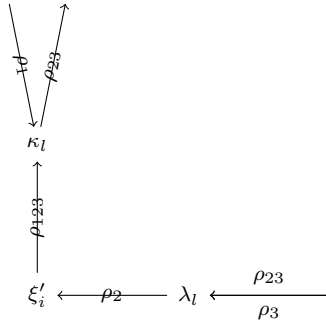
come from cases where in fig. 12a the arrow going out of κ_ℓ (into κ_ℓ , respectively) has a ρ_{23} (ρ_1 , respectively). Similarly, on the right side, the two red arrows (three blue arrows, respectively) come from cases where in fig. 12a the arrow going into λ_ℓ has a ρ_{23} (ρ_3 , respectively).

Then we cancel the two green arrows and the pink arrow in the middle and arrive at fig. 12c. Note the joint at $y_3 \otimes \kappa_\ell$, which is boxed in fig. 12c, can now be identified with the corresponding part of $KtD(C^{flip})$, which would look like the joint itself.

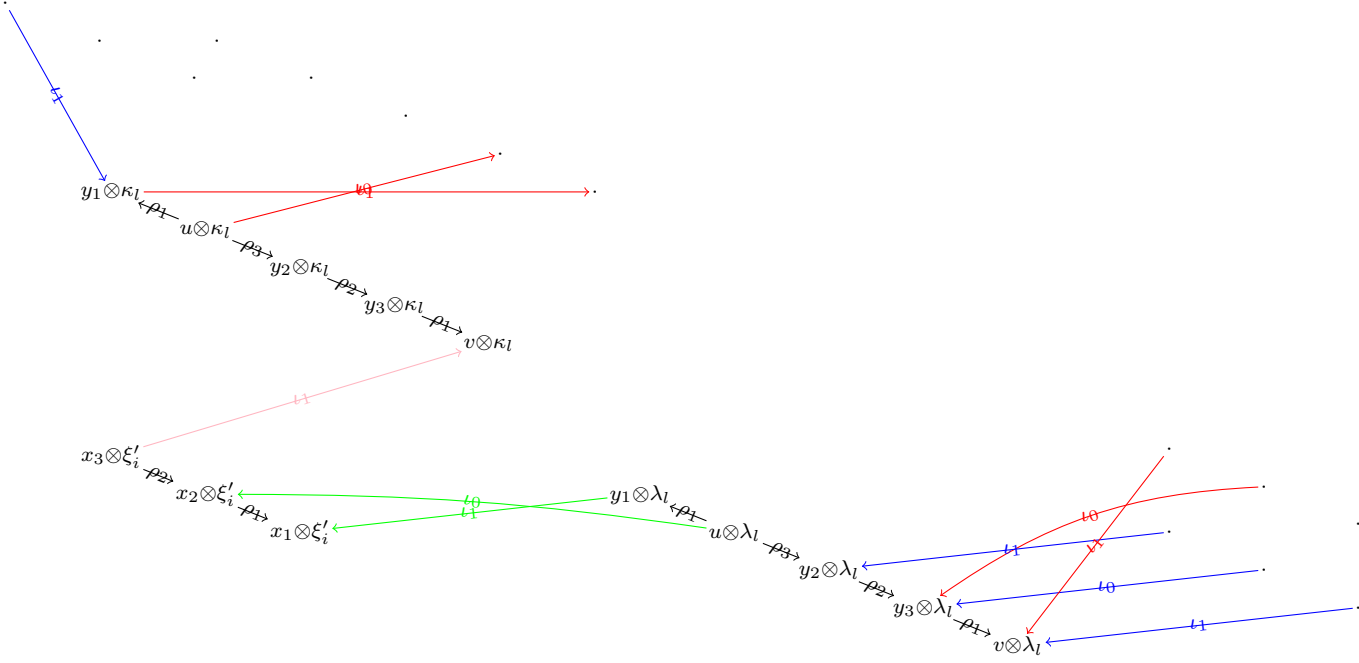
If either of the two possibilities in fig. 12a is ρ_{23} , as above, we observe that cancellation of either set of two red arrows in fig. 12c agree with the cancellations we performed for a string of ρ_{23} 's in section 3.3.1. This shows chains containing ρ_{23} 's at $y_3 \otimes \kappa_\ell$ in $H \boxtimes KtD(C)$ (fig. 13a) exactly match corresponding chains in $KtD(C^{flip})$, which would again look like the joint itself.

Now we deal with the four cases of overlapping joints involving a lower left joint, see the last four diagrams of fig. 11. First, for the case in fig. 11e, we combine fig. 12b with fig. 4b. All generators involving λ_ℓ are identified with those with λ_1 , and the two sets of two green arrows and two sets of three blue arrows are respectively identified. We perform the same two sets of cancellations and arrive at fig. 13b. It can be identified with the corresponding part in $KtD(C^{flip})$.

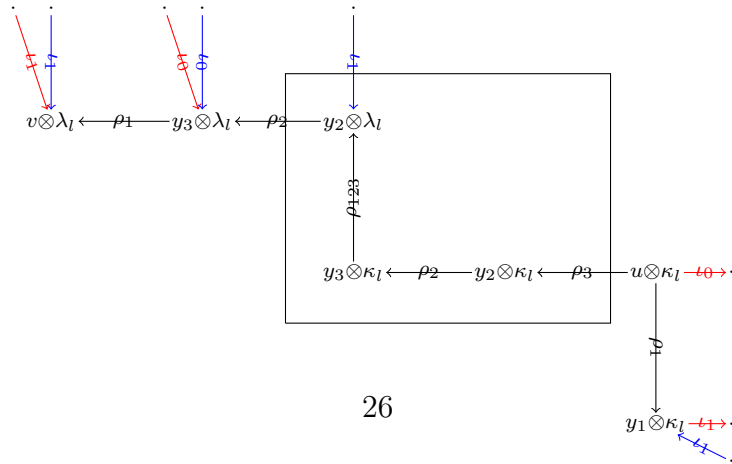
The remaining three cases in fig. 11f, fig. 11g, and fig. 11h can be proved in a similar fashion: we combine two tensor products of H with corresponding joints shown in this and above sections, then identify overlapping generators and arrows, and finally observe that cancellations done separately for each joint can be combined without conflicting. We provide the results in fig. 13c, fig. 14a, and fig. 14b, and omit further details.



(a) Lower left joint at ξ'_i

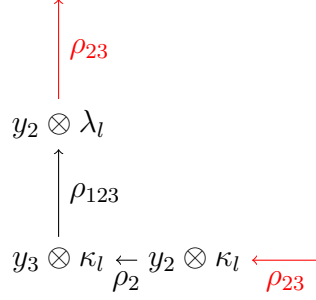


(b) Tensor product with H .

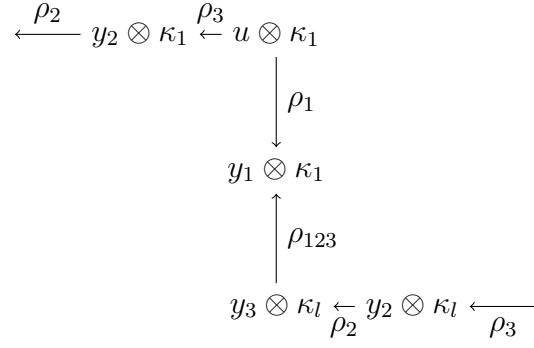


(c) After cancellation.

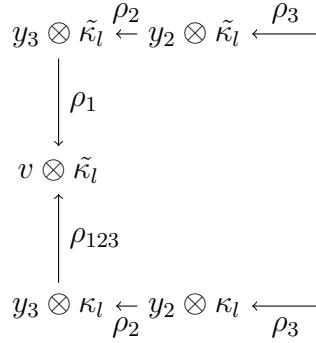
Figure 12: Lower left joint



(a) Cases where either arrow at ξ'_i have length more than 1

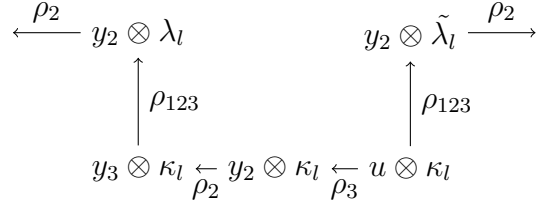


(b) A lower left joint connected to a upper right joint

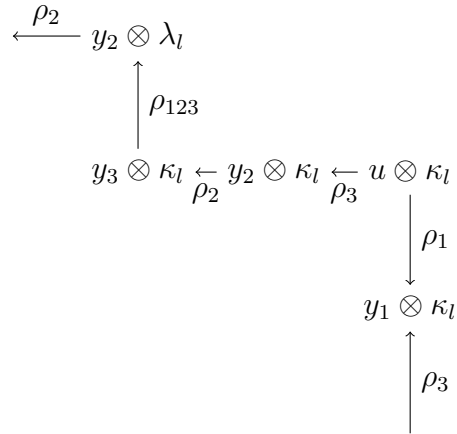


(c) A lower left joint connected to a lower right joint. $\tilde{\kappa}_\ell$ refers to the κ_ℓ from the lower right joint.

Figure 13: Lower left joint



(a) A lower left joint connected to a upper left joint. $\tilde{\lambda}_\ell$ refers to the λ_ℓ from the upper left joint.



(b) A lower left joint connected to a upper right joint in a different way

Figure 14: Lower left joint

3.3.6 The unstable chain

So far we have avoided ξ_v , ξ_h , and the unstable chain between them in our discussion. We now argue that the proof for the unstable chain can be reduced to the cases discussed above.

Recall when $n < 2\tau(K)$, the unstable chain takes form:

$$\xi'_v \xrightarrow{\rho_1} \mu_1 \xleftarrow{\rho_{23}} \cdots \xleftarrow{\rho_{23}} \mu_k \xleftarrow{\rho_{23}} \mu_{k+1} \xleftarrow{\rho_{23}} \cdots \xleftarrow{\rho_{23}} \mu_m \xleftarrow{\rho_3} \xi'_h,$$

where $m = 2\tau(K) - n \geq 3$, by assumption.

If $\xi_v = \xi_h$, the unstable chain appears as in fig. 15a. Now, H acts on the string of ρ_{23} 's by flipping them into the opposite direction. At generator ξ'_v , the arrows are exactly like a upper right joint in fig. 4a in section 3.3.2, so the arrows are also flipped. The proof there carries over to show that H tensoring with the unstable chain in $KtD(C)$ matches the unstable chain in $KtD(C^{flip})$.

Now suppose $\xi_v \neq \xi_h$. We observe that the unstable chain is the end of chains for vertical arrows spliced with the end of chains for horizontal arrows. For this reason, we can interpret arrows at ξ'_v and ξ'_h as joints we have already discussed.

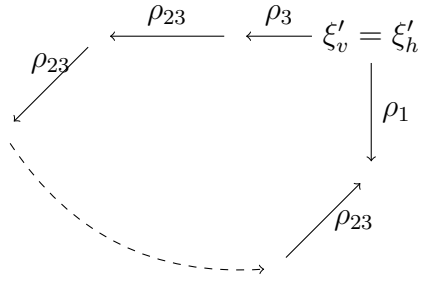
For example, arrows at ξ'_v match exactly to a upper left joint as in fig. 6a if ξ_v has an incoming arrow, and a upper right joint as in fig. 4a if ξ_v has an outgoing arrow, see fig. 15b.

Similarly, arrows at ξ'_h match exactly to a lower right joint as in fig. 9a if ξ_h has an incoming arrow, and a upper right joint as in fig. 4a if ξ_h has an outgoing arrow, see fig. 15c.

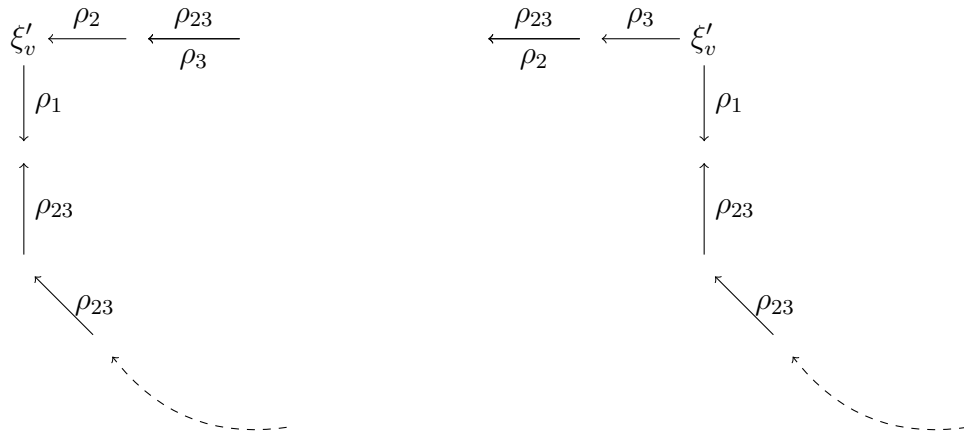
Now the proof is easy. In the case where ξ_v has an incoming horizontal arrow, the corresponding generator ξ_v^{flip} in C^{flip} is a generator with no horizontal arrow and an incoming vertical arrow, so its corresponding generator $\xi_v^{flip'}$ in $KtD(C^{flip})$ has a lower right joint. Now H acts by matching the upper left joint at ξ'_v to the lower right joint at $\xi_v^{flip'}$ as discussed in section 3.3.3. The case where ξ_h has an incoming vertical arrow works backwards using the H action discussed in section 3.3.4.

Similarly, the correspondence between the case where ξ_v has an outgoing horizontal arrow and the case where ξ_h has an outgoing vertical arrow can be shown with the H action discussed in section 3.3.2.

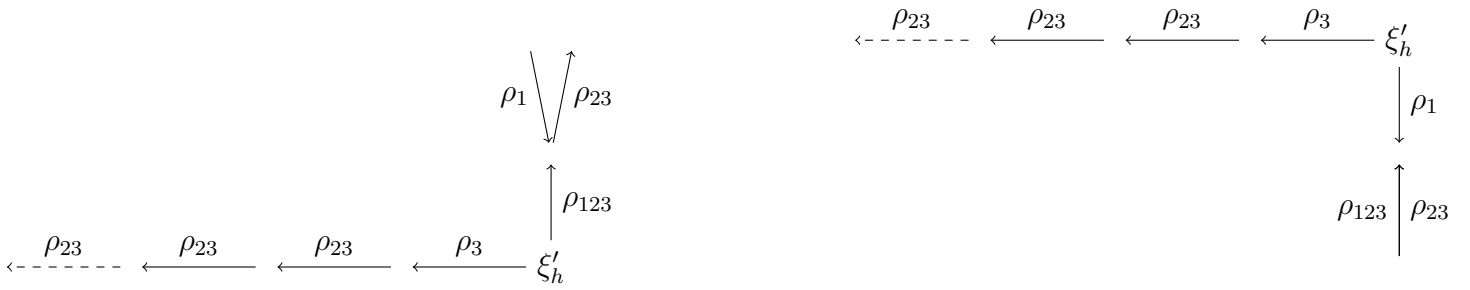
Now we have finished the proof.



(a) Unstable chain in the case where $\xi_v = \xi_h$



(b) Joints at ξ'_v



(c) Joints at ξ'_h

Figure 15

3.4 Proof of the General Case

Now we prove Proposition 2 without the extra assumption of C being simultaneously horizontally and vertically simplified. Instead we only assume it is reduced and horizontally simplified as in Proposition 2. We use Theorem 3, the base-free version of the algorithm from \widehat{CFD} to CFK^- .

First, we give an example of Theorem 3. Suppose we have a knot Floer complex C as in fig. 16a.



- (a) Generators a and b have Alexander filtration level 1. Alexander filtration level of generators c and e is 0, and that of d is -1.
- (b) The Alexander filtration levels for a, b, c, d and e are -1, -1, 0, 1, and 0, respectively.

Figure 16

Applying Theorem 3 with $n = 7$ yields $KtD(C)$ as in fig. 17.

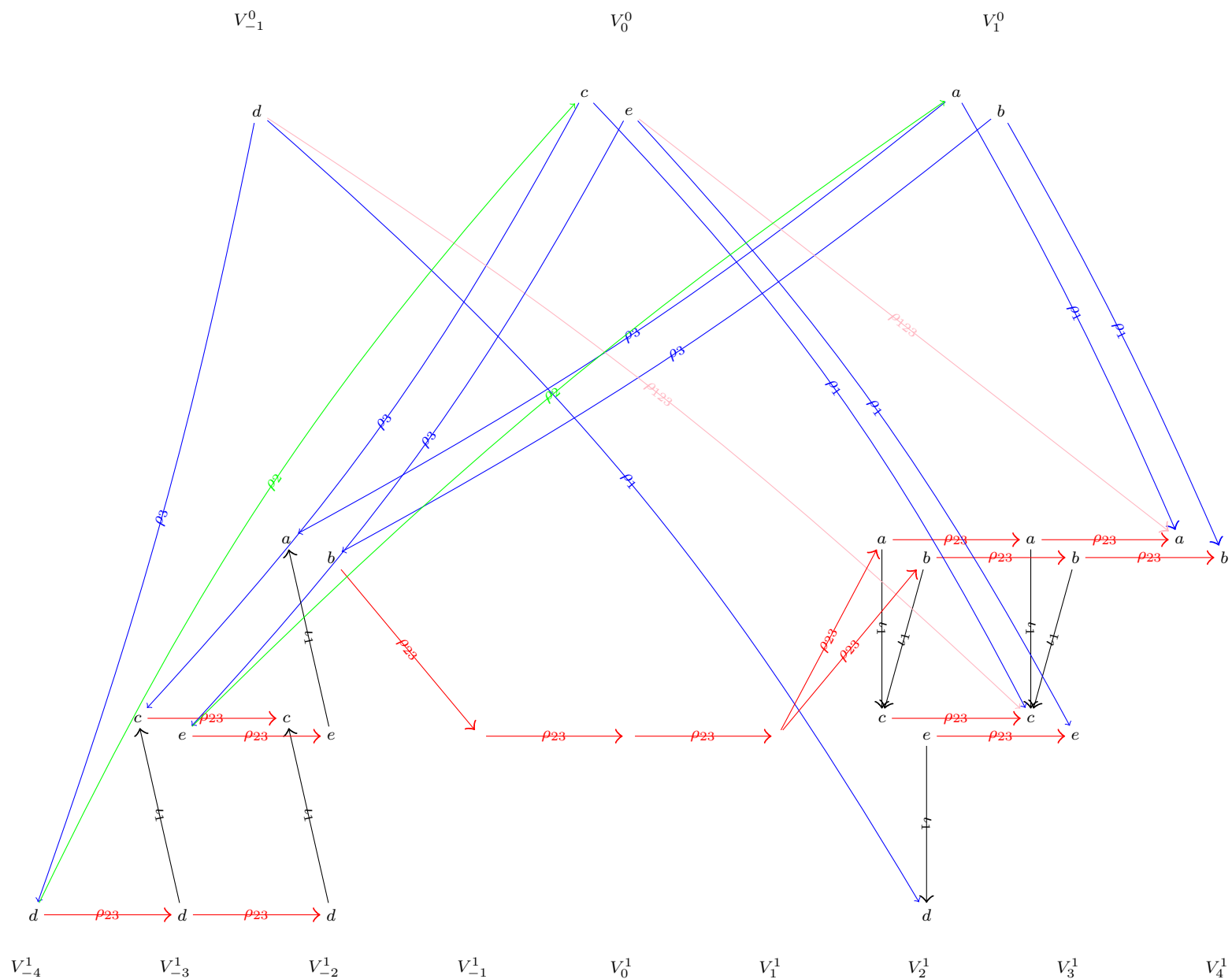


Figure 17

If we apply the procedures in Theorem 3 to C^{flip} , which is shown in fig. 16b, we get the complex $KtD(C^{flip})$ shown in fig. 18. We now rearrange the generators by rotating both V^0 and V^1 180 degrees to arrive at fig. 19.

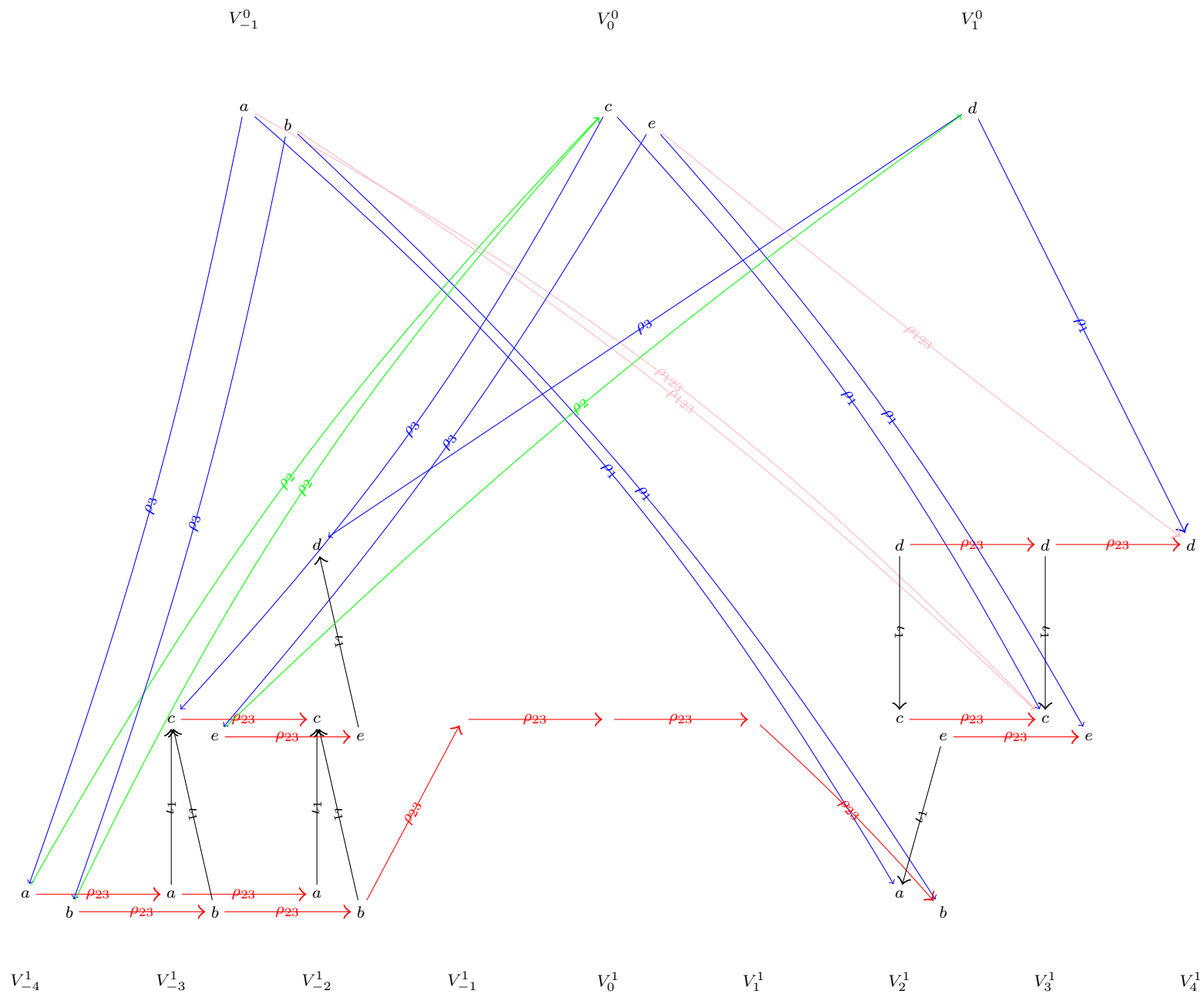


Figure 18

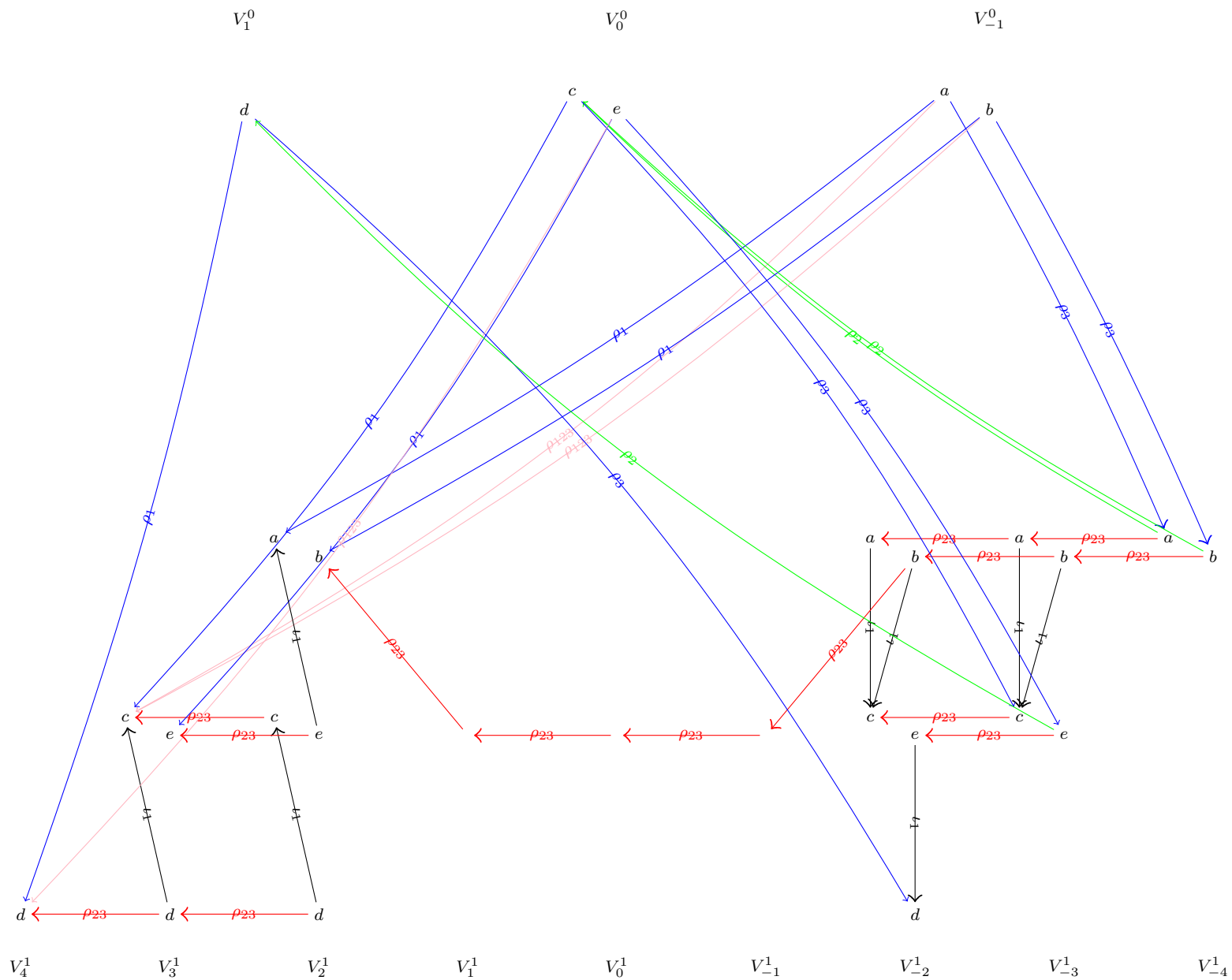


Figure 19

Comparing the result with $KtD(C)$, we see the generators can be completely identified between them. So are the differentials without non-trivial algebra elements. All arrows with ρ_{23} 's have their directions reversed, except those between the central string of ρ_{23} 's and the two full copies of C immediately next to the string. ρ_1 's and ρ_3 's switch sides. With careful choices of n and the Alexander filtrations on C^{flip} , we can proof this is in general true.

We first set the convention to display KtD 's as we did in the example above: V^0 on top of V^1 , with smaller s on the left. Within V_s^1 , we arrange generators vertically according to Alexander level and we call them "in the same column". On the horizontal direction, put generators corresponding to the same generator in C on the same horizontal line. They are denoted by the same letters in the diagrams. Hence they are connected by horizontal arrows with ρ_{23} 's. We say they are on the same "row".

We state here the identifications between various sub/quotient complexes of C and C^{flip} :

$$\begin{aligned}(C(\leq s), \partial_w) &\cong (C^{flip}(\geq -s), \partial_z) \\ (C(\geq s), \partial_z) &\cong (C^{flip}(\leq -s), \partial_w)\end{aligned}$$

Lemma 2. *Let h be the maximal Alexander filtration level and ℓ be the minimal Alexander filtration level of C . Let $t = \max\{h, -\ell\}$. We choose $n = 4t + 3$ for both $KtD(C)$ and $KtD(C^{flip})$ from now on. Note that with the choice of n , we simply have $V_s^1 = \mathbb{F}_2, |s| \leq t$, $V_{t+1}^1 = (C, \partial_z)$, and $V_{-t-1}^1 = (C, \partial_w)$. We call the latter two (and other V_s^1 such that $V_{s \geq t+1}^1 = (C, \partial_z)$ and $V_{s \leq -t-1}^1 = (C, \partial_w)$) the "full copies".*

Now $KtD(C^{flip})$ can be directly constructed from $KtD(C)$ as follows. We describe this construction graphically to facilitate the proof later.

- *Keep all the generators in $KtD(C)$.*
- *Relabel V_s^0 with V_{-s}^0 and V_s^1 with V_{-s}^1 for all s , but still arrange them graphically the same way, i.e. s decreases now from left to right.*
- *Reverse the direction of all ρ_{23} 's, except those between the central sequence of ρ_{23} 's and the two full copies on either side of the sequence.*
- *Replace the rest of ρ_{23} 's (those between the sequence and the two full copies) with isomorphism-inducing chain maps in the opposite direction.*
- *At every generator in V^0 , switch the arrows ρ_1 and ρ_3 coming out.*

- Remove all existing ρ_2 and ρ_{123} .
- For $s < -t$, $V_s^1 = C(\geq -s - \frac{n-1}{2})$ is missing $C(-s - 1 - \frac{n-1}{2})$ if compared to the column on its left $V_{s+1}^1 = C(\geq -s - 1 - \frac{n-1}{2})$. If there exists an downward arrow $x \rightarrow y$ in V_{s+1}^1 , where $y \in C(-s - 1 - \frac{n-1}{2})$, then add an arrow ρ_2 from $x \in V_s^1$ to $y \in V_{s+\frac{n+1}{2}}^0$.
- For every generator $x \in V^0$, if there exists an (downward) outgoing arrow $x \rightarrow y$ of length 1 in V_{-t}^1 , then add an arrow ρ_{123} from $x \in V^0$ to the unique generator y at the leftmost position of its row.

Proof. This proof is nothing more than applying the procedure in Theorem 3 to C^{flip} and comparing with $KtD(C)$.

We call the D-module constructed this way X and argue X can be identified with $KtD(C^{flip})$.

Per our construction, $\forall s$, $(V_s^0 \text{ of } X) \cong (V_{-s}^0 \text{ of } KtD(C)) \cong C(-s) \cong C^{flip}(s) \cong (V_s^0 \text{ of } KtD(C^{flip}))$, as \mathbb{Z} -filtered chain complexes over \mathbb{F}_2 .

$\forall s \leq -\frac{n}{4} = -t - 0.75$, $(V_s^1 \text{ of } X) \cong (V_{-s}^1 \text{ of } KtD(C)) \cong (C(\geq -s - \frac{n-1}{2} = -s - 2t - 1), \partial_z) \cong (C^{flip}(\leq s + 2t + 1), \partial_w) \cong (V_s^1 \text{ of } KtD(C^{flip}))$, as \mathbb{Z} -filtered chain complexes over \mathbb{F}_2 .

$\forall |s| \leq \frac{n}{4} = t + 0.75$, $(V_s^1 \text{ of } X) \cong \mathbb{F}_2 \cong (V_s^1 \text{ of } KtD(C^{flip}))$

$\forall s \geq \frac{n}{4} = t + 0.75$, $(V_s^1 \text{ of } X) \cong (V_{-s}^1 \text{ of } KtD(C)) \cong (C(\leq -s + \frac{n-1}{2} = -s + 2t + 1), \partial_w) \cong (C^{flip}(\geq s - 2t - 1), \partial_z) \cong (V_s^1 \text{ of } KtD(C^{flip}))$, as \mathbb{Z} -filtered chain complexes over \mathbb{F}_2 .

Now we look at arrows with nontrivial algebra elements on them. First, arrows with ρ_1 and ρ_3 . Per our construction, $D_1 : V_s^0 \rightarrow V_{s+\frac{n-1}{2}}^1 \text{ of } KtD(C)$ become $D_3 : V_{-s}^0 \rightarrow V_{-s-\frac{n-1}{2}}^1 \text{ of } X$ and $D_3 : V_s^0 \rightarrow V_{s-\frac{n-1}{2}}^1 \text{ of } KtD(C)$ become $D_1 : V_{-s}^0 \rightarrow V_{-s+\frac{n-1}{2}}^1 \text{ of } X$. So

$$\begin{aligned}
(D_1 : V_{-s}^0 \rightarrow V_{-s+\frac{n-1}{2}}^1 \text{ of } X) &\cong (D_3 : V_s^0 = C(s) \rightarrow V_{s-\frac{n-1}{2}}^1 = C(\leq s) \text{ of } KtD(C)) \\
&\cong (i : C(s) \rightarrow C(\leq s)) \cong (i : C^{flip}(-s) \rightarrow C^{flip}(\geq -s)) \\
&\cong (D_1 : V_{-s}^0 = C^{flip}(-s) \rightarrow V_{-s+\frac{n-1}{2}}^1 = C^{flip}(\geq -s) \text{ of } KtD(C^{flip}))
\end{aligned}$$

Similarly,

$$\begin{aligned}
(D_3 : V_{-s}^0 \rightarrow V_{-s-\frac{n-1}{2}}^1 \text{ of } X) &\cong (D_1 : V_s^0 \rightarrow V_{s+\frac{n-1}{2}}^1 \text{ of } KtD(C)) \\
(i : C(s) \rightarrow C(\geq s)) &\cong (i : C^{flip}(-s) \rightarrow C^{flip}(\leq -s))
\end{aligned}$$

$$(D_3 : V_{-s}^0 = C^{flip}(-s) \rightarrow V_{-s-\frac{n-1}{2}}^1 = C^{flip}(\leq -s))$$

The newly added ρ_2 's are exactly done to match those in $KtD(C^{flip})$. They are:

$$\begin{aligned} (D_2 : V_{-s}^1 = C(\geq -s - \frac{n-1}{2}) \xrightarrow{\partial_z} C \xrightarrow{\pi} V_{-s-\frac{n+1}{2}}^0 = C(-s - \frac{n+1}{2})inX) \\ \cong (C^{flip}(\leq s + \frac{n-1}{2}) \xrightarrow{\partial_w} C^{flip} \xrightarrow{\pi} C^{flip}(s + \frac{n+1}{2})), \end{aligned}$$

which matches D_2 in $KtD(C^{flip})$.

Similar logic goes for the newly added ρ_{123} 's. They are:

$$\begin{aligned} (D_{123} : V_{-s}^0 = C(s) \xrightarrow{\partial_z} C(s-1) \rightarrow V_{-s+\frac{n+1}{2}}^1 = C(\leq s-1)inX) \\ \cong (C^{flip}(-s) \xrightarrow{\partial_w} C(-s+1) \rightarrow C(\geq -s+1)) \cong (D_{123}inKtD(C^{flip})) \end{aligned}$$

D_{23} : The new ρ_{23} 's are: for $s > \frac{n}{4}$,

$$\begin{aligned} D_{23} : V_s^1 = C(\leq -s + \frac{n-1}{2}) \rightarrow V_{s+1}^1 = C(\leq -s-1 + \frac{n-1}{2}) \\ \cong C^{flip}(\geq s - \frac{n-1}{2}) \rightarrow C^{flip}(\geq s - \frac{n+1}{2}), \end{aligned}$$

which matches those in $KtD(C^{flip})$. The rest of the ρ_2 's similarly match. □

Now that we have proved the differences between $KtD(C)$ and $KtD(C^{flip})$ are fairly “local”, we proceed to prove that tensoring with H and canceling carefully transform $KtD(C)$ into $KtD(C^{flip})$.

Each generator in $V^0 \subset KtD(C)$ corresponds to three generators in $KtD(C) \boxtimes H$ and each one in $V^1 \subset KtD(C)$ corresponds to five generators in $KtD(C) \boxtimes H$, see fig. 20a. An arrow with ρ_1 ($\rho_3, \rho_2, \rho_{23}, \rho_{123}$, respectively) corresponds to arrows in $KtD(C) \boxtimes H$ in fig. 20b (fig. 20c, fig. 20d, fig. 20e, fig. 20f respectively.)

Now we can finally take the tensor $KtD(C) \boxtimes H$ and perform cancellation. We first state that cancellation will be done in the order discussed below.

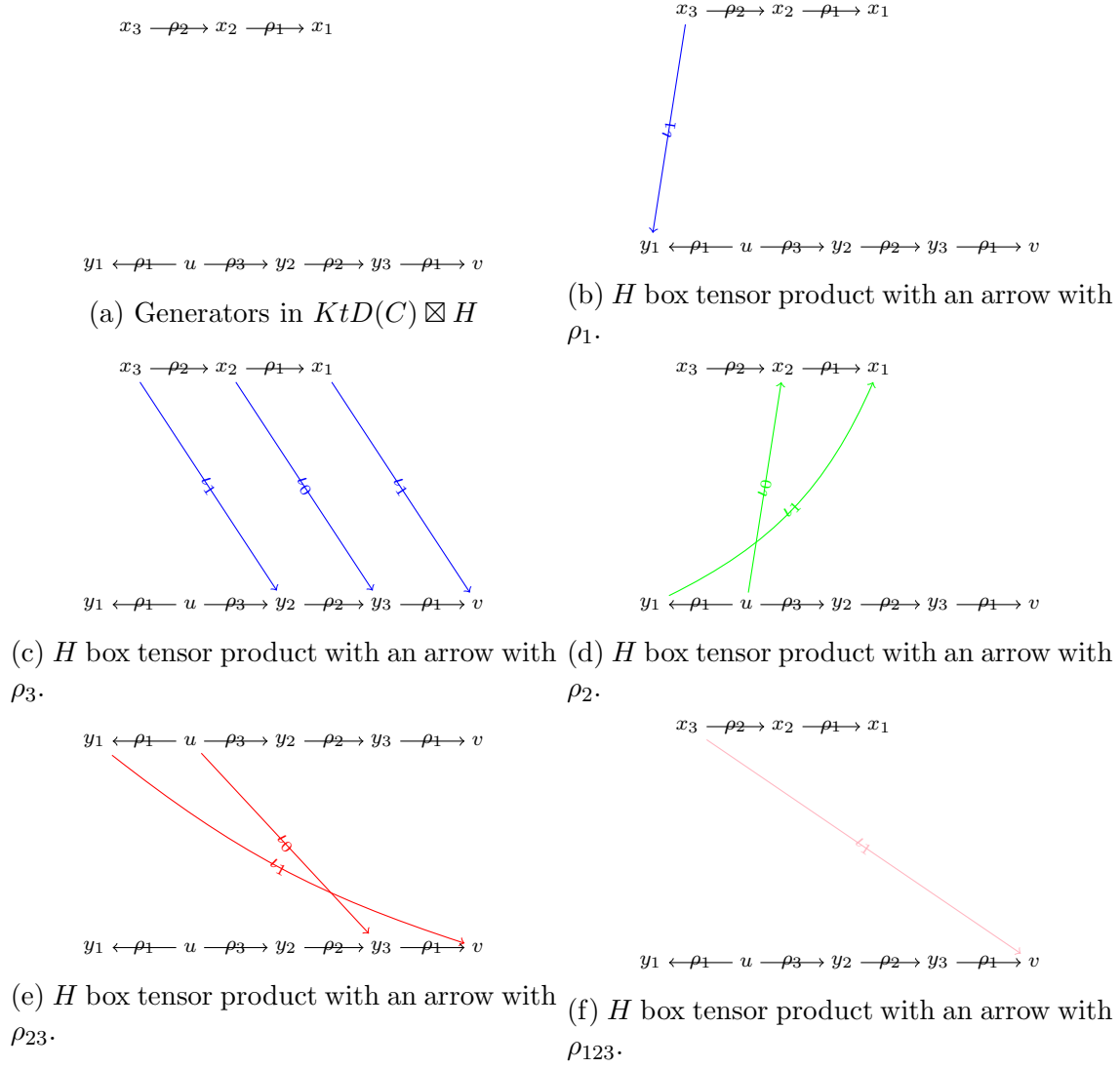


Figure 20: Tensoring for generators and arrows

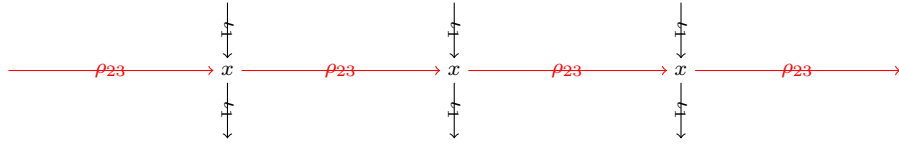
3.4.1 Right-hand side middle part of rows in V^1

We start from the “right” side of V^1 . For any row of generator x connected by a string of ρ_{23} ’s in $\oplus_{s>t} V_s^1$, we first look at the middle part, i.e., excluding the leftmost one in the full copy and rightmost one where there might be ρ_1, ρ_{123} coming in, see fig. 21a. Black arrows into and out of x ’s represent the potential and possibly multiple arrows of ∂_z within this column.

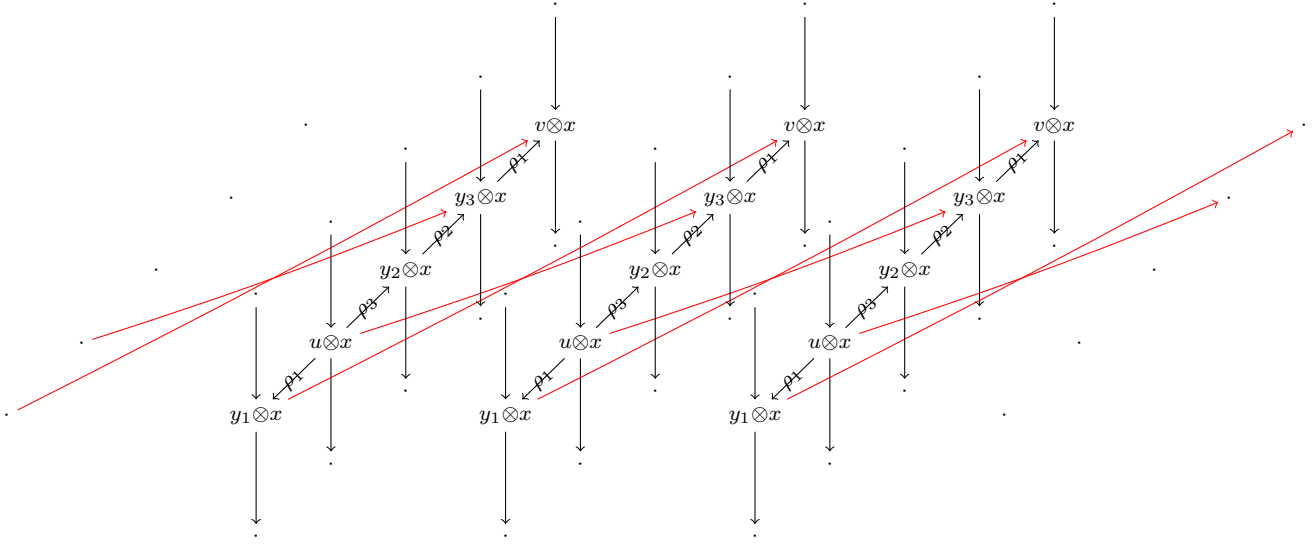
It looks like fig. 21b in the tensor product. Each string of y_1, u, u_2, y_3, v corresponds to a single generator before. Black arrows coming in and out of them represent the tensor result of potential arrows of ∂_z .

We first cancel the red arrows from y_1 to v , arriving at fig. 21c. We keep the arrows resulted from cancellation in shape of zigzags to make it easier to see how they were generated.

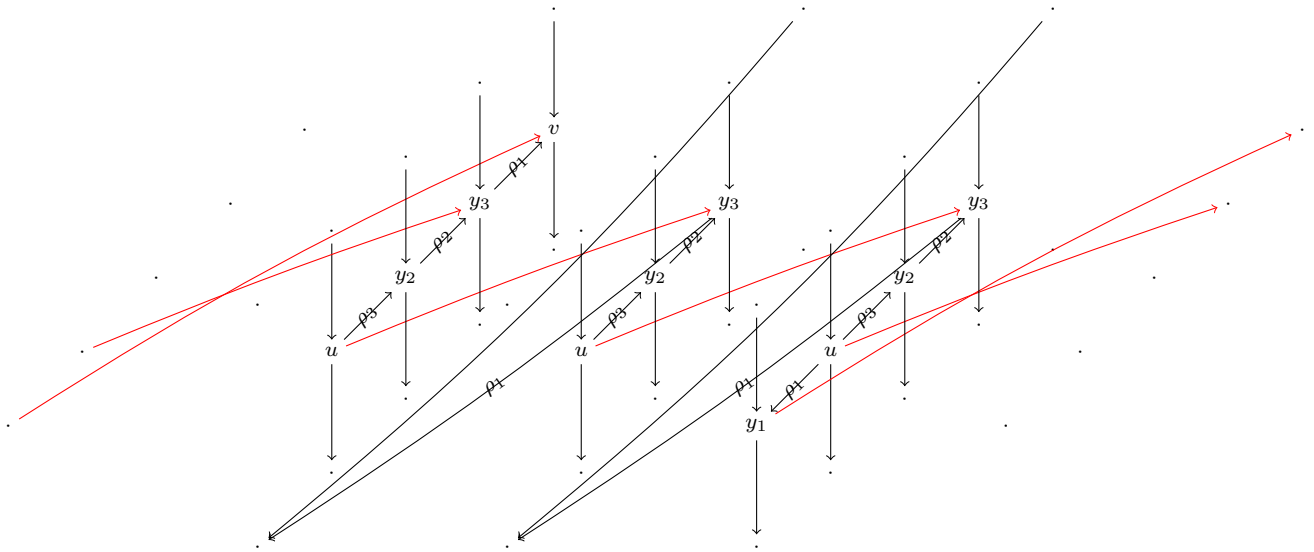
Then canceling red arrows from u to y_3 yields fig. 22a. Note the new ρ_{23} ’s in the opposite direction between the y_2 ’s. They and the ρ_{23} ’s between them match the generators in $KtD(C^{flip})$ in the way described by lemma 2. In general, throughout the proof, y_2 ’s in the tensor product are the generators that will survive and match to generators in $KtD(C^{flip})$. We repeat the process above for all such rows in the “right” side. In this process, some undesirable arrows appear as a side effect and we argue that such arrows will not survive at the end. For example, the (potential) arrow (marked by # in fig. 22a) coming from a v_i above in the middle column and going to a y_1 below in the left column. When we follow this process in the row containing the v_i , we will cancel a red arrow going into v_i , meaning any arrow coming out of v_i will be discarded. Similar logic goes to the rest of the undesirable arrows; they either come out v ’s and y_3 ’s, which are the target of arrows to be cancelled, or enter y_1 ’s and u ’s, which are the origin of arrows to be cancelled. One exception will be when the u ’s below are at rightmost positions of their row, where they won’t have red arrowing coming out to be cancelled. We remark that, in such cases, only the (possibly multiple) arrow marked by $*$ could survive, while the others will be gone because of their origins being targets of arrows to be cancelled. Note in each row, such a surviving arrow can only appear once for each downward arrow in ∂_z . See fig. 22b for the final product. We emphasize that we perform cancellation described here across all applicable places first before moving on to other parts of the module.



(a) Middle part of a row.



(b)



(c)

Figure 21: Middle part of a row.

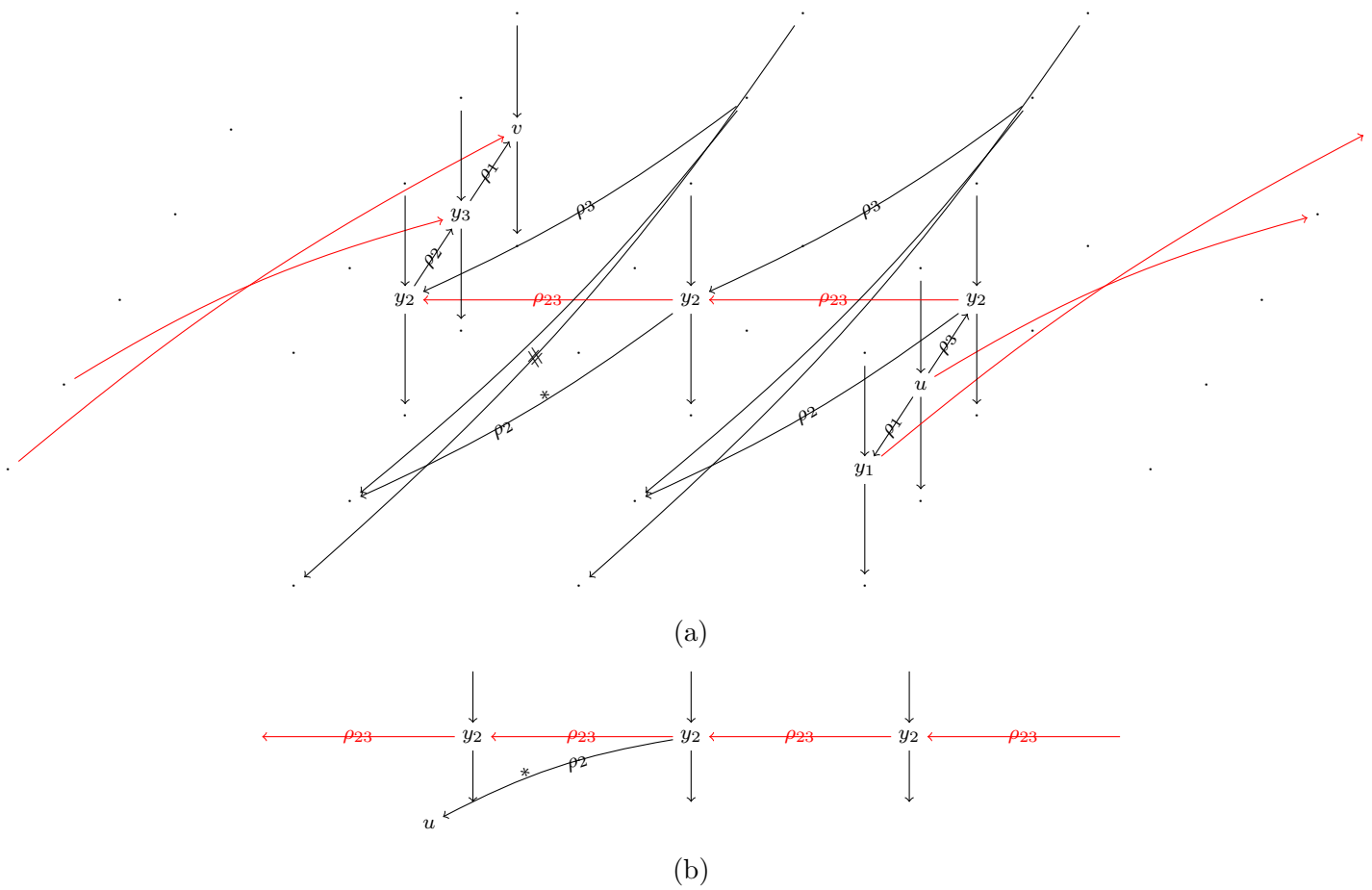
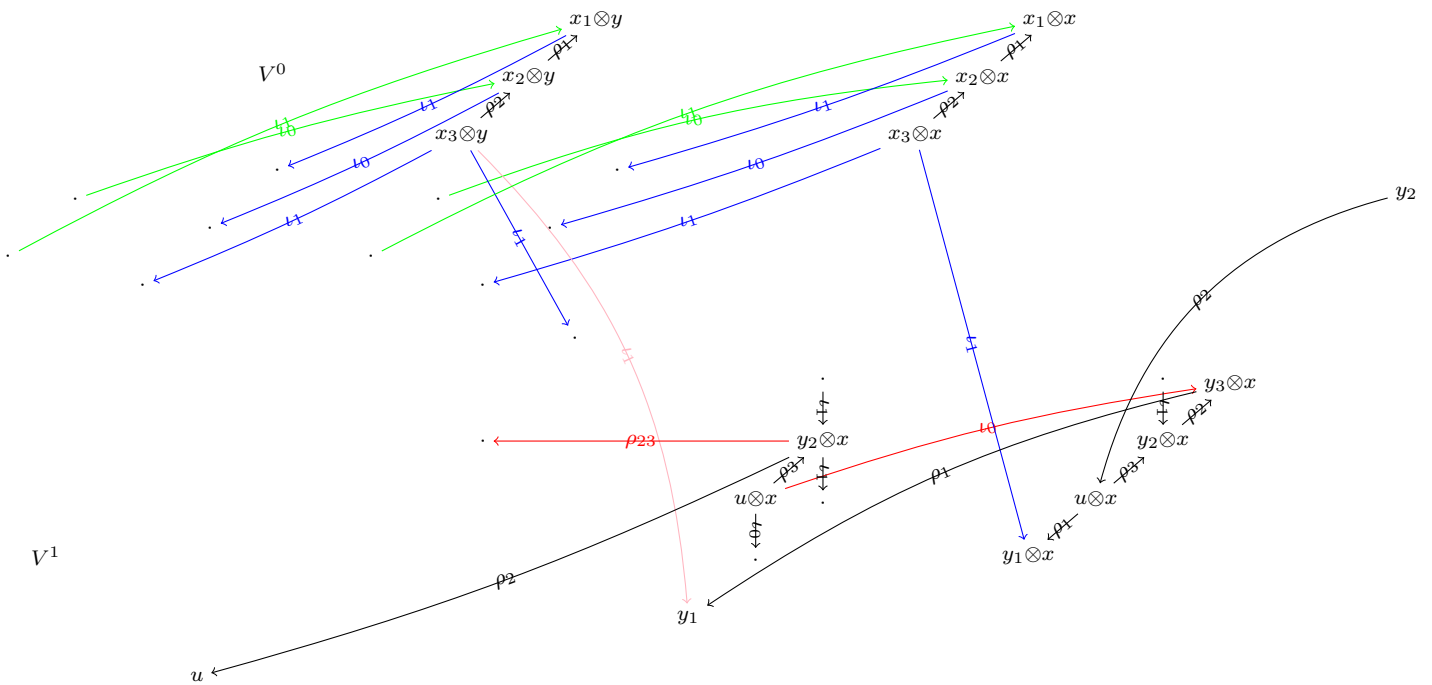


Figure 22: Middle part of a row.

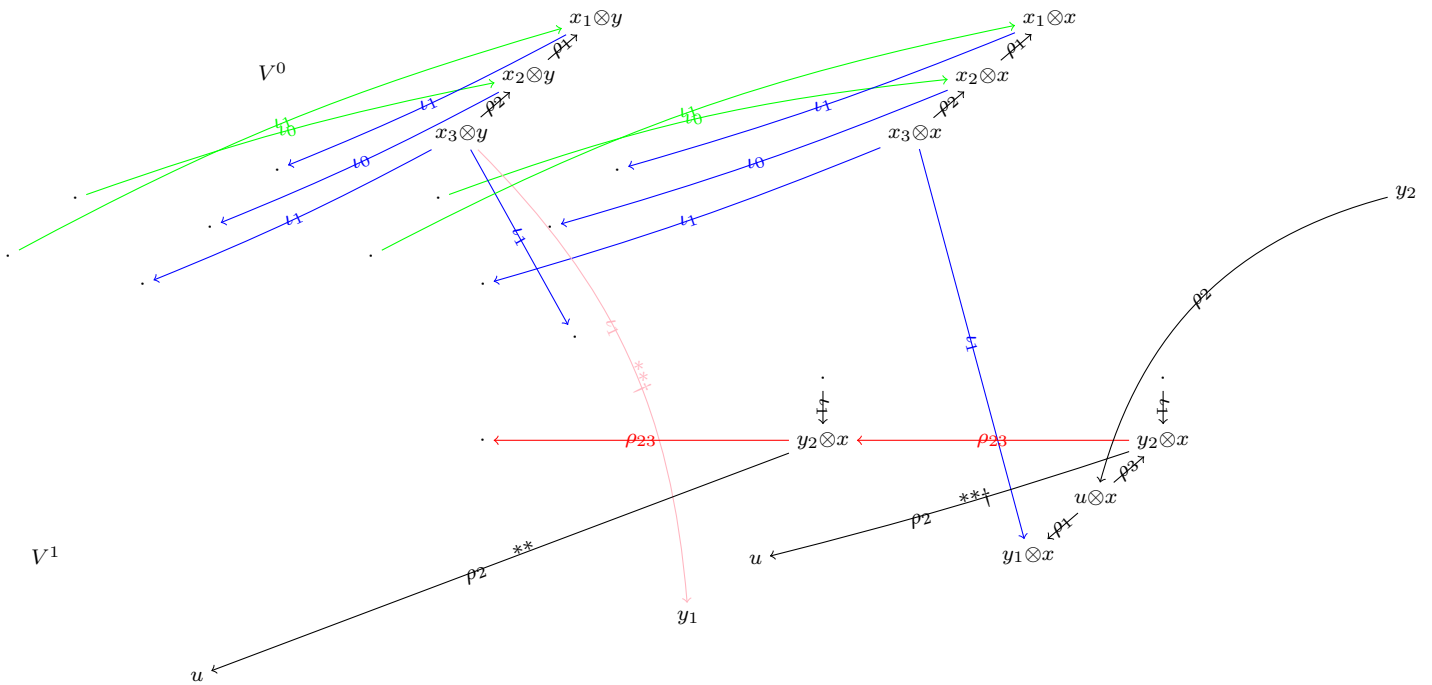
3.4.2 Right-hand side rightmost end of rows in V^1

We look at the rightmost positions of rows, see fig. 23a. The blue, green, and pink arrows represent ρ_1 , ρ_3 , and potential and possibly multiple ρ_2 and ρ_{123} . It corresponds to fig. 23b in the tensor product. Again the black arrows are potential arrows from tensoring with ∂_z . Note that there is only one connecting to the right string of generators. There are not any going out because this is the right most position and only y_2 has black arrow(s) coming in because we have performed the cancellation described in section 3.4.1 on rows above. Regarding the left set of generators, there are only three of them and one incoming black arrow for the same reason. The black arrows marked by $*$ are the potential side effect of cancellation performed to rows above, see section 3.4.1.

Next we cancel the two red arrows in the middle successively, see fig. 24a and fig. 24b. Now ∂_z into y_2 's and the ρ_{23} among them match those in $KtD(C^{flip})$. As for the messy additional arrows, we keep them in mind and bring them into shape later. We make the observation that the potential side effect ρ_2 arrows going to u 's and the pink arrow going to a y_1 in row below (all marked by $**$ in fig. 24b) only exist if they enter u 's in the rightmost end of their rows. In the case of the $**\dagger$ arrows, they exist only if x has a length one ∂_z arrow. Even though they enter another right-most position in another row, we clearly see that they do not interfere with the procedure in this section applied there. So we are safe to say that we can perform these cancelations at all right-most ends of rows. An exception is when a row has only one generator, which can only happen at the bottom row. We discuss that case in section 3.4.3.



(a)



(b)

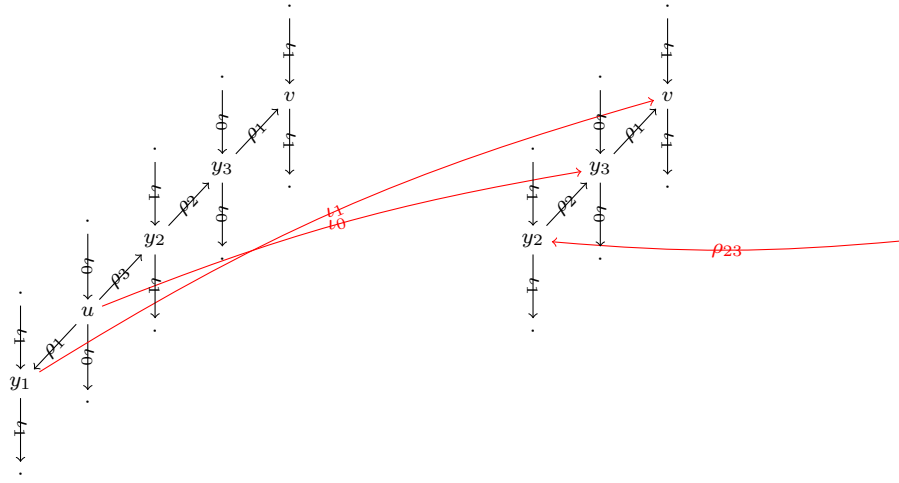
Figure 24: Rightmost position of a row

3.4.3 Right full copy

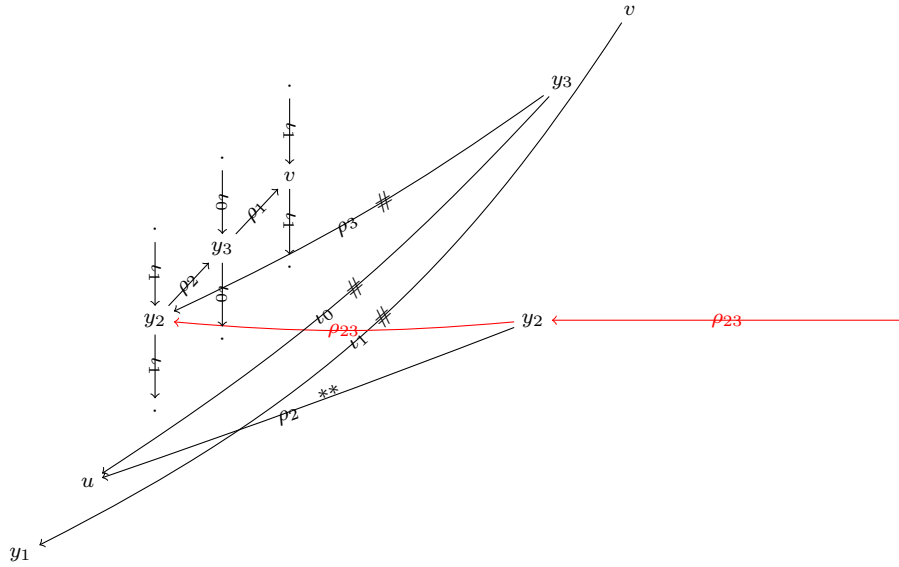
fig. 25a shows the part of the full copy in the tensor product. As we have done twice, we cancel the red arrows resulting in fig. 25b. Note the arrows marked with # will be gone after we apply these cancellations in the rows above. Their existence does not interfere with the cancellation above, as they come out of targets of cancelable arrows. Such arrows coming from rows below would not have interfered here either. Disregarding those arrows, we arrive at fig. 25c. Again the arrow marked with ** only exists if it goes into a u in rightmost position, which in this case can only be the bottom row. fig. 26a depicts the bottom row which has only one generator, with the potential ** arrow shown. The blue arrow comes from tensoring with ρ_1 . Note there will not be any pink arrows from tensoring with potential ρ_{123} , because this generator has the lowest Alexander grading.

The only arrows connecting to the full copy are those from the map $i : \mathbb{F}_2 \rightarrow C$, which induces isomorphism in homology. The map i must take the generator e of \mathbb{F}_2 to some $\sum_j x_j \in C$. The full picture of the full copy looks like fig. 26b. The set of three generators on the left corresponds to e . Because we can simply treat the middle string of ρ_{23} 's as we did in the simple case, a ρ_{23} coming out of y_2 is obviously the result of those cancellations. Only x_1 and x_2 are shown for simplicity.

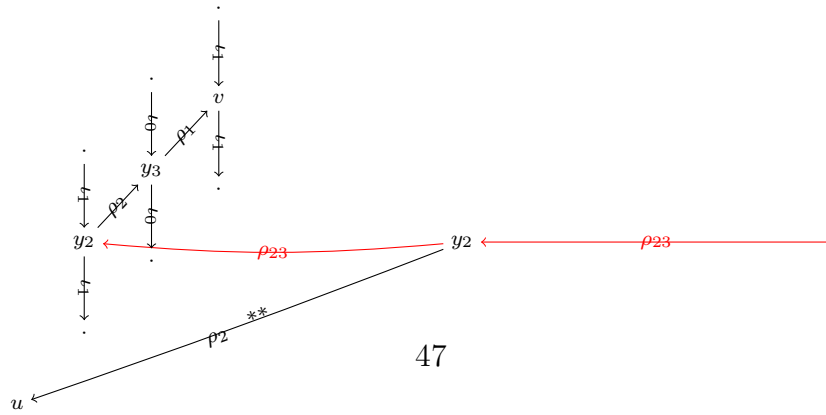
A map inducing isomorphism in homology in the opposite direction of i must take $x_j \rightarrow e$ for some j and all other generators of C to 0. So in order to match with $KtD(C^{flip})$, we need one ρ_{23} from one of the x_i 's to e . We first cancel arrow marked by #1 and arrive at fig. 27a. Now cancel the arrow marked by #2 and arrive at fig. 27b. We then look to rid all the v 's in this picture. The set of v 's and the differentials among them make a chain complex C_v over \mathbb{Z}_2 slightly different from C . We observe that if we perform the change of basis $x_1 \rightarrow \sum_j x_j$ on C and then the resulting complex minus generator $\sum_j x_j$ is isomorphic to C_v . Following the fact that (C, ∂_z) is homotopy equivalent to \mathbb{Z}_2 and $\sum_i x_i$ is the generator of the homology, C_v is homotopy equivalent to \emptyset . This means that there is a homotopy equivalence on the current stage of the module that exactly gets rid of all the v 's. A similarly constructed homotopy equivalence gets rid of all the y_3 's. The final result matches the full copy of $KtD(C^{flip})$, see fig. 28a.



(a)



(b)



(c)

Figure 25: The right full copy

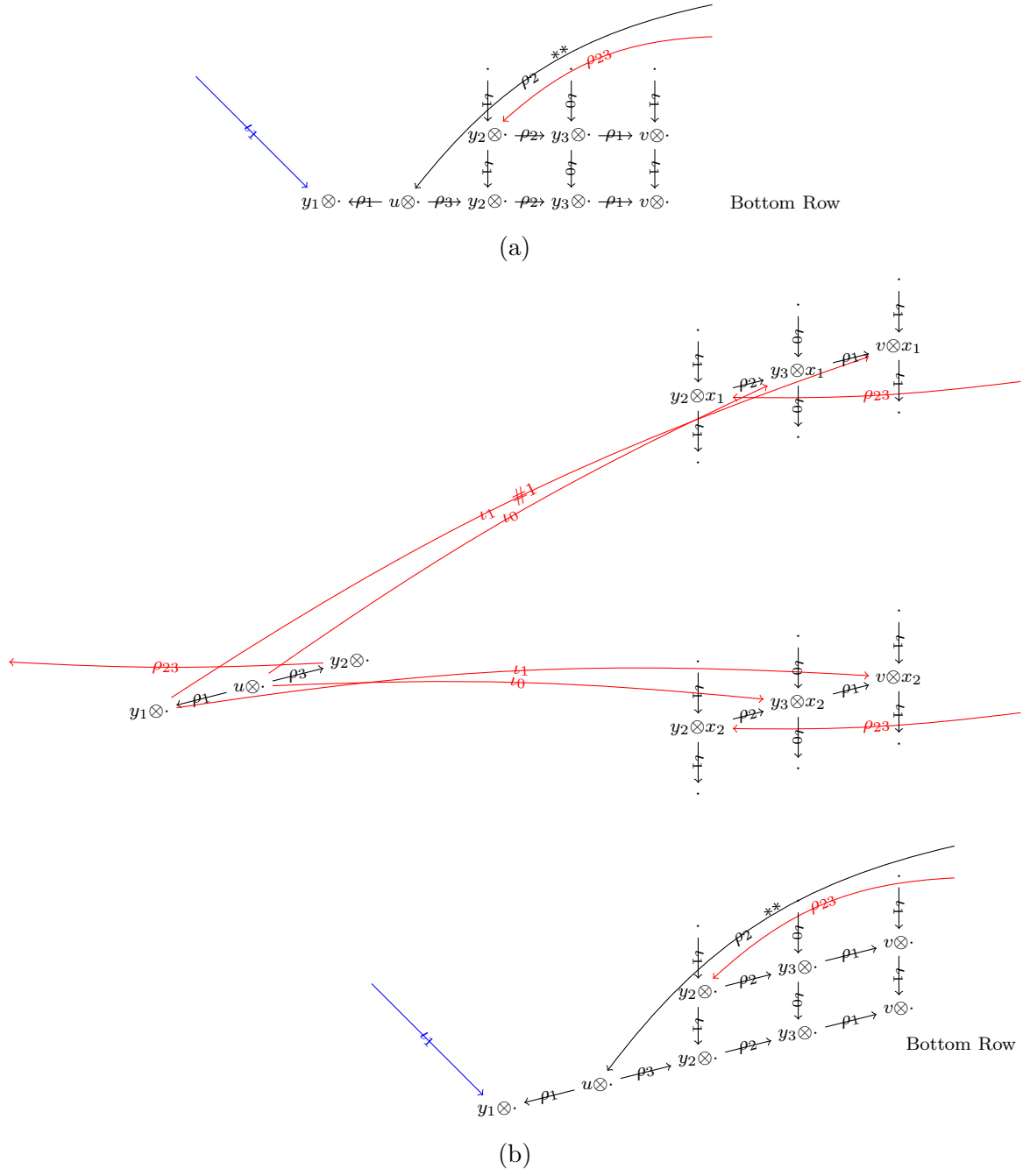
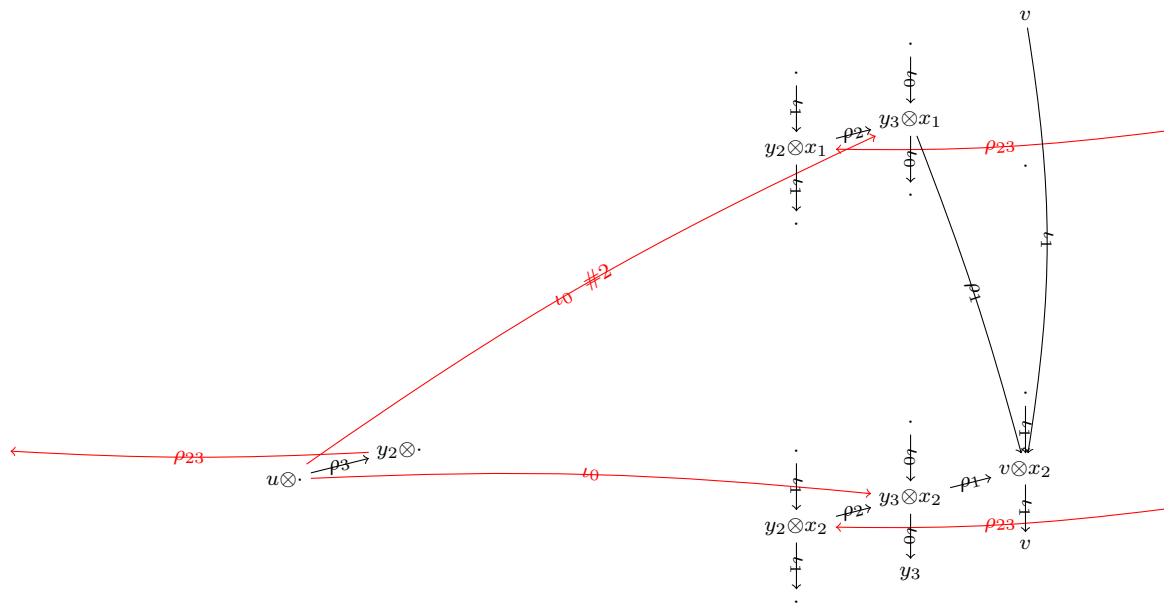
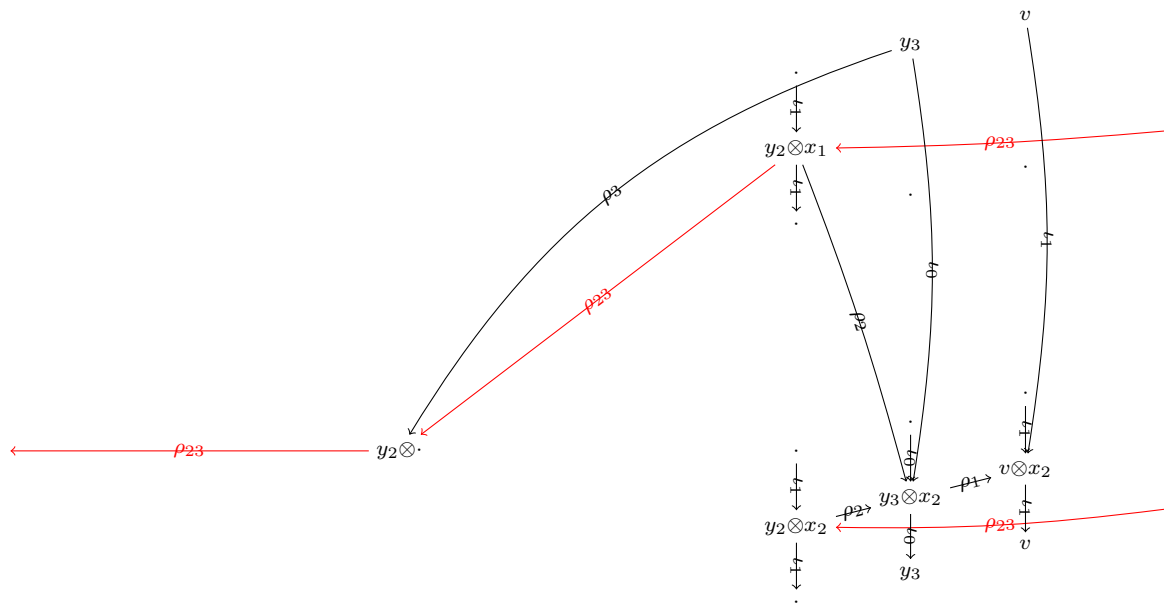


Figure 26: The right full copy



(a)



(b)

Figure 27: The right full copy

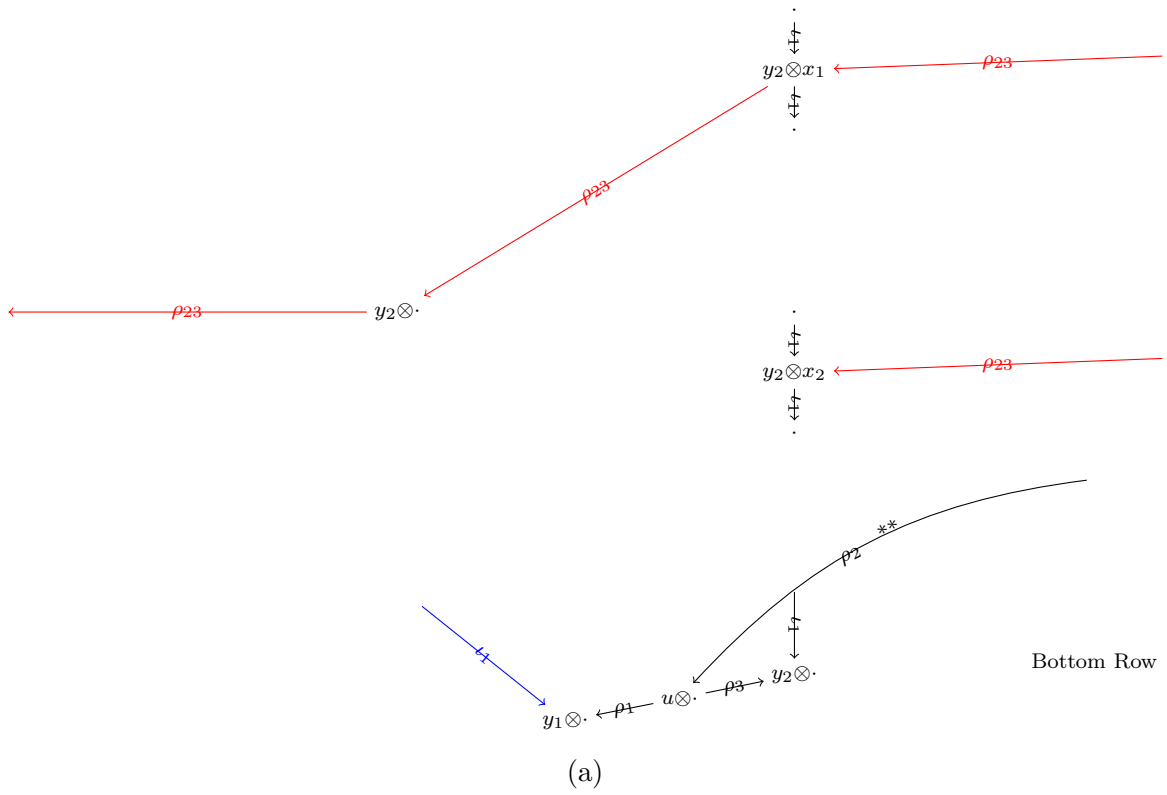


Figure 28: The right full copy

3.4.4 Left-hand side middle part of rows in V^1

We switch to the left-hand side. Recall that we assumed that C is horizontally-simplified. This means generators in (C, ∂_w) come in pairs except one generator, which we call ξ_h to be consistent with the simplified case. Two generators in each pair are connected by one arrow. A typical pair $a \rightarrow b$ in $KtD(C)$ is displayed in fig. 29a. The green arrow with ρ_2 goes to $b \in V^0$. Per Theorem 3, it always appear one column to the left of the left-most $a \rightarrow b$ arrow in $(C(\leq s), \partial_w)$ for some s . The dots are only place holders to demonstrate that the length of the arrow is 3.

In the “middle” part of this long string, away from the left-most $a \rightarrow b$ arrow and the right-most full copy, the cancellation in the tensor product is just a simplified case of the process described in section 3.4.1, see fig. 30a and fig. 30b.

The unpaired ξ_h constitutes a single string of ρ_{23} ’s in $KtD(C)$, whose middle part can be dealt with in the same manner. The result is a string of ρ_{23} ’s in the opposite direction, matching $KtD(C^{flip})$.

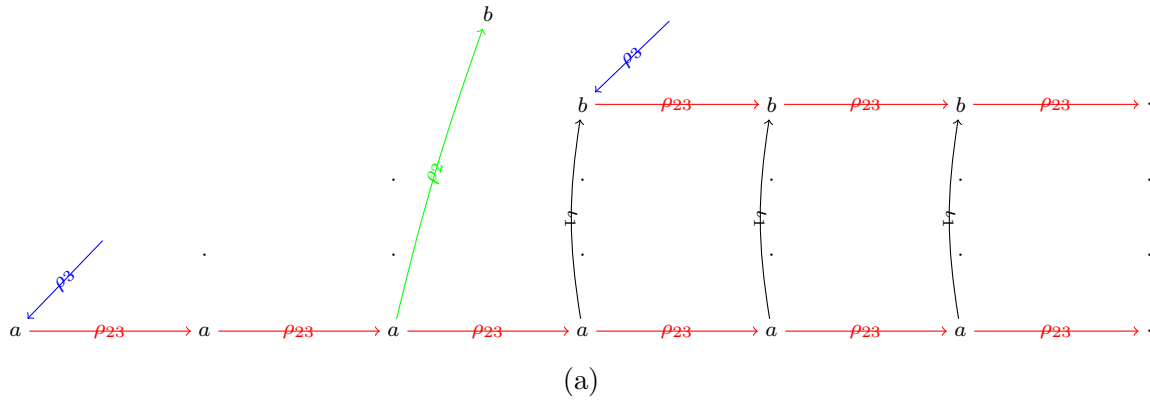


Figure 29: Lefthand side middle part of rows in V^1

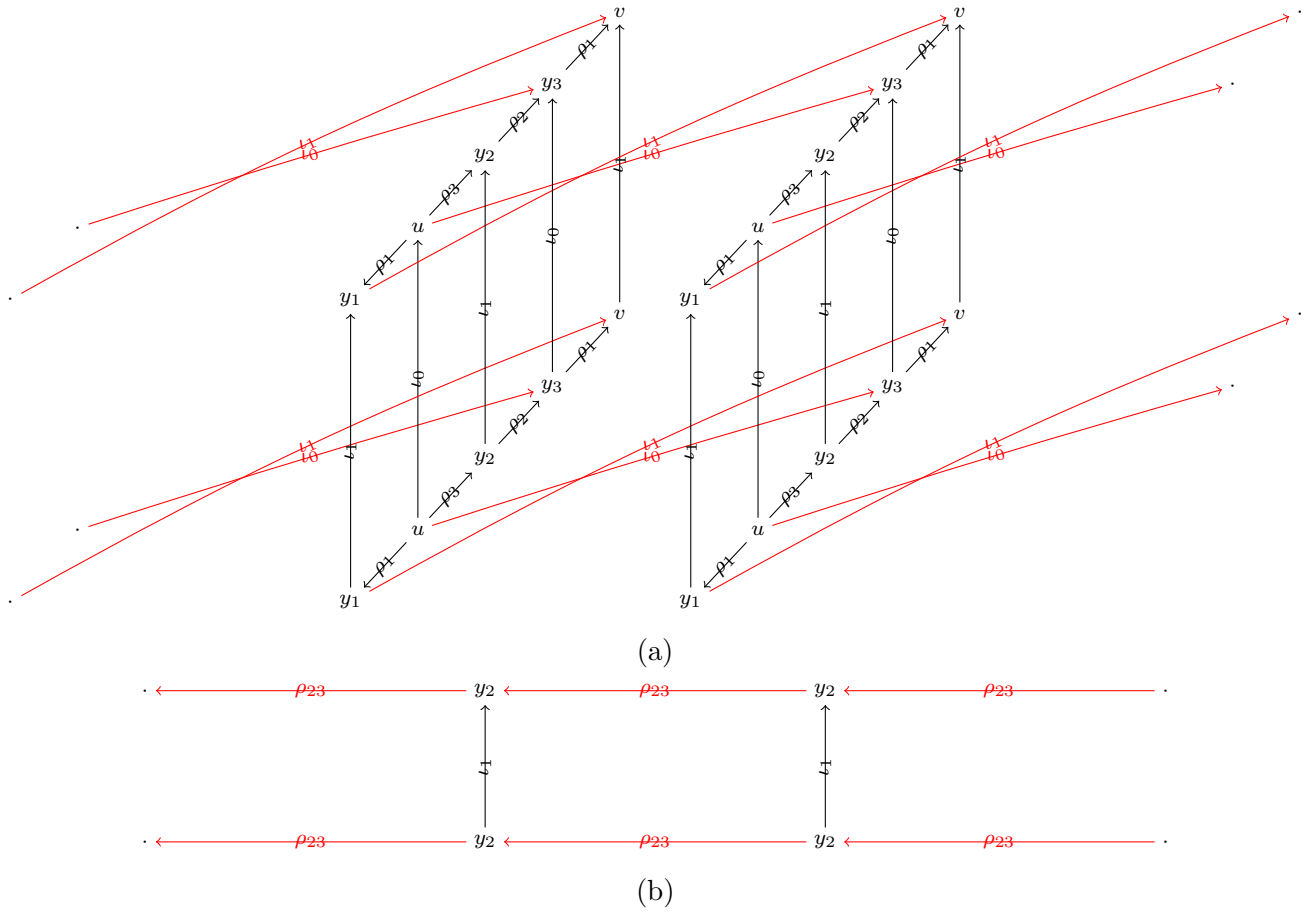


Figure 30: Left-hand side middle part of rows in V^1

3.4.5 V^0

In this section we look at tensoring at V^0 where outgoing ρ_1 and ρ_3 connect to the left-most positions of the left-hand side and right-most positions of the right-hand side, see fig. 31. We first assume the arrow $a \rightarrow b$ has length more than 1. This means that on the left of fig. 31, the position where the green arrow comes out is not the left most position, where the blue ρ_3 comes in. It also means that there won't be any other length one ∂_w arrow connecting to a or b , so there is not any pink ρ_{123} 's to the right side of this diagram.

Taking the tensor and keeping in mind all the previous cancellation we have done, especially in section 3.4.2 and fig. 24b, we arrive at fig. 32. We first cancel the two pair of red arrows in the same fashion we have always done. We also cancel the two blue arrows from $x_1 \rightarrow v$, then the two blue arrows from $x_2 \rightarrow y_3$, resulting in fig. 33. The cancelation of the eight arrows so far are simple and generated no new arrows. Note the green arrows are now gone.

Next, we cancel the two pair of red arrows on the left and rearrange the y_1 's and u 's on the right side to the top, see fig. 34a. Next, we cancel the two blue arrows $x_3 \rightarrow y_1$ on the top, see fig. 34b.

Now the picture looks very much like $KtD(C^{flip})$ described in lemma 2; For each generator, its y_2 takes its place. ρ_{23} 's are reversed. ∂_z and ∂_w are intact. For each generator x , its u at the right-most position in the right side takes the place of x in V^0 . ρ_1 and ρ_3 are switched. Let us take a closer look at the green arrows with ρ_2 and marked by $*$ in this section. Say the a has an incoming $c \rightarrow a$ in ∂_z . As seen in section 3.4.1, the green arrow $*$ with ρ_2 comes from c 's y_2 in one column to the right. In other words, if a downward ∂_z arrows arrives at a generator a at a right-most position from a generator c above, then there is a ρ_2 arrow coming out of the y_2 to c 's right and going into the bottom a 's u , which takes the place of the old $a \in V^0$ now. This matches exactly to the green arrows of $KtD(C^{flip})$ described in lemma 2. The green arrows marked by $**$ exist for the exact same reasons, except from the origin's point of view. They exist only when they are going into a rightmost position, which must be the rightmost position of one row below, as they themselves are at rightmost positions. We again observe that these green arrows never interacted with the cancellation done in this section, so we are safe to say that we the cancellations generalize to all applicable part.

The case depicted in the diagrams is that $a \rightarrow b$ has length 2, the case that it has length more than 2 is similar.

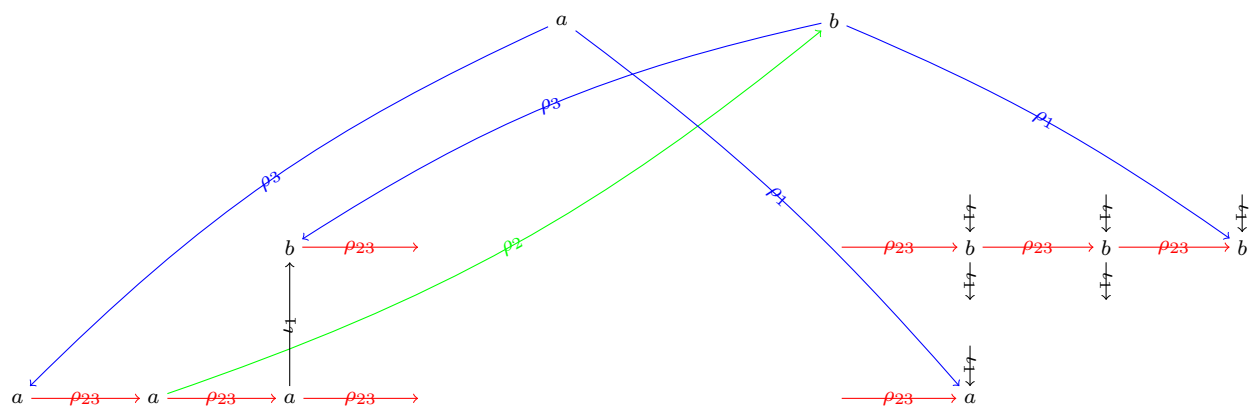
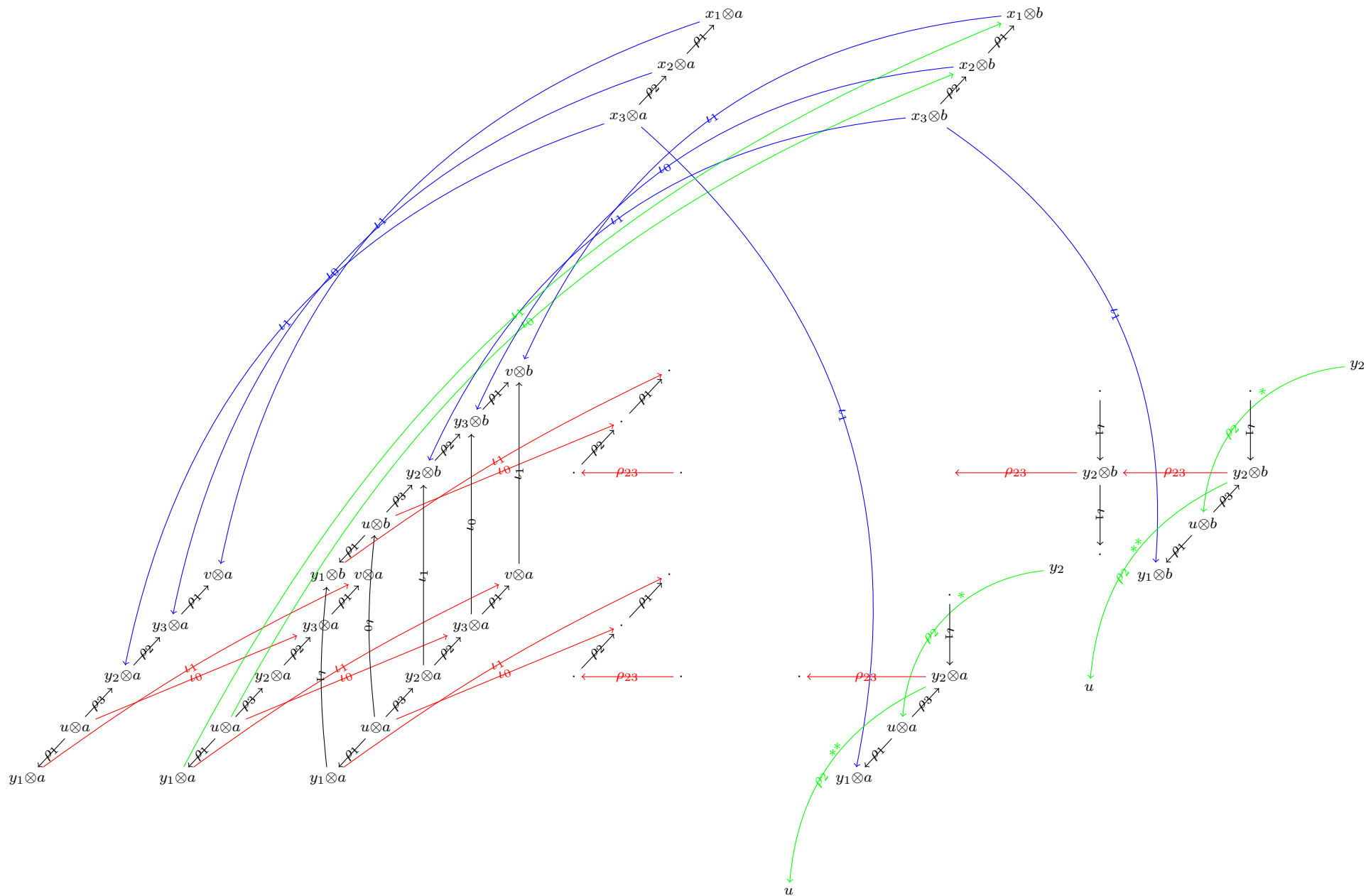
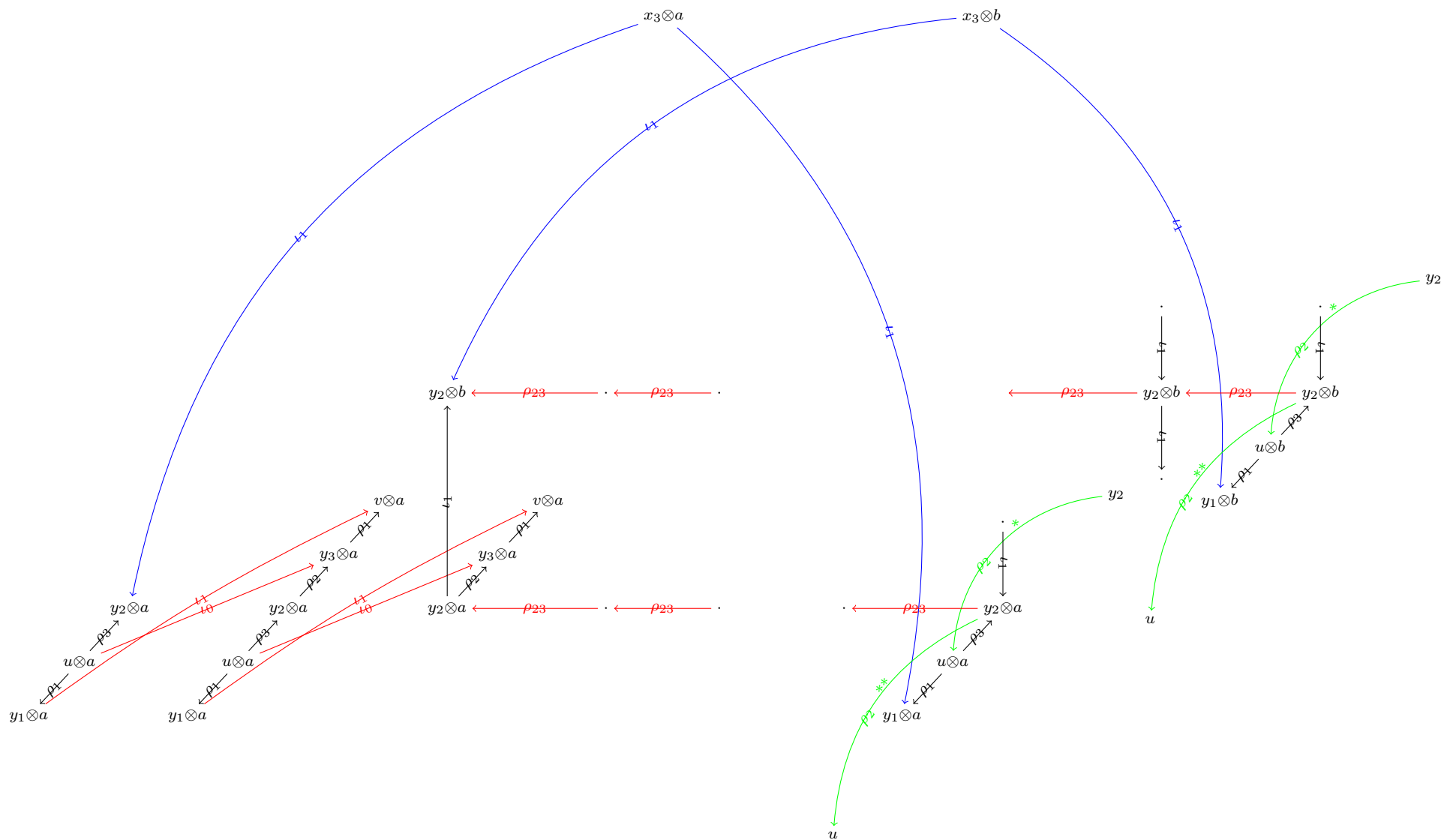
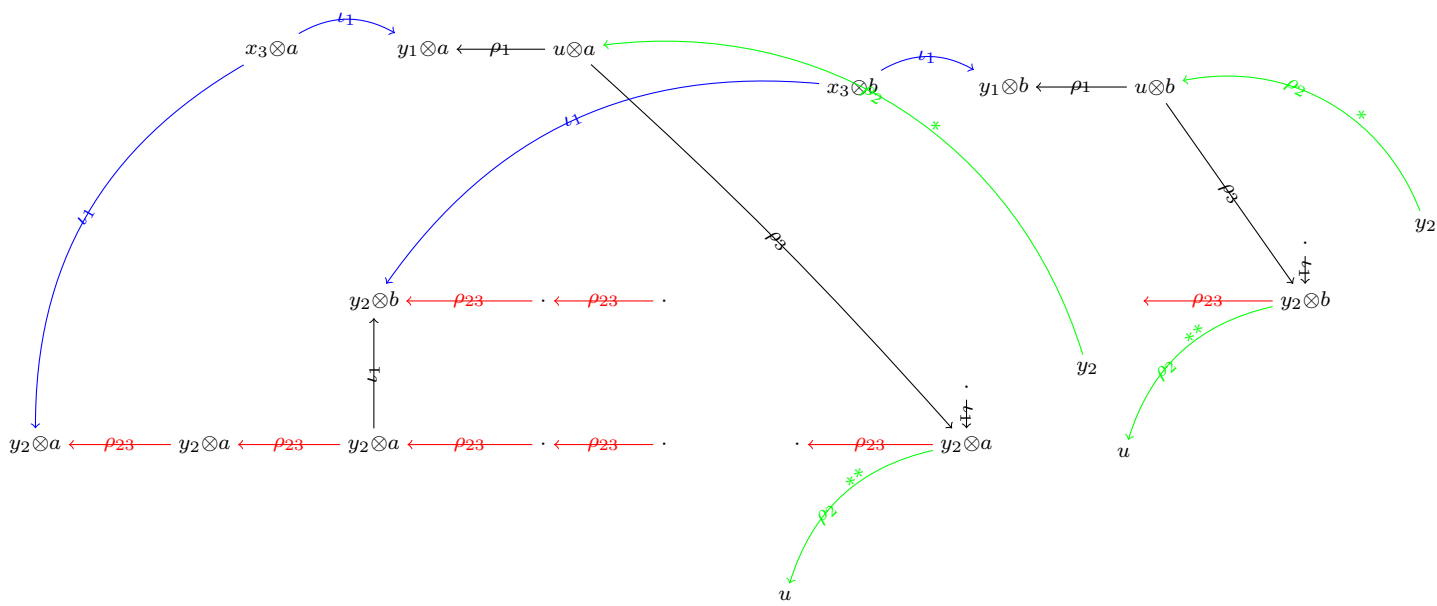


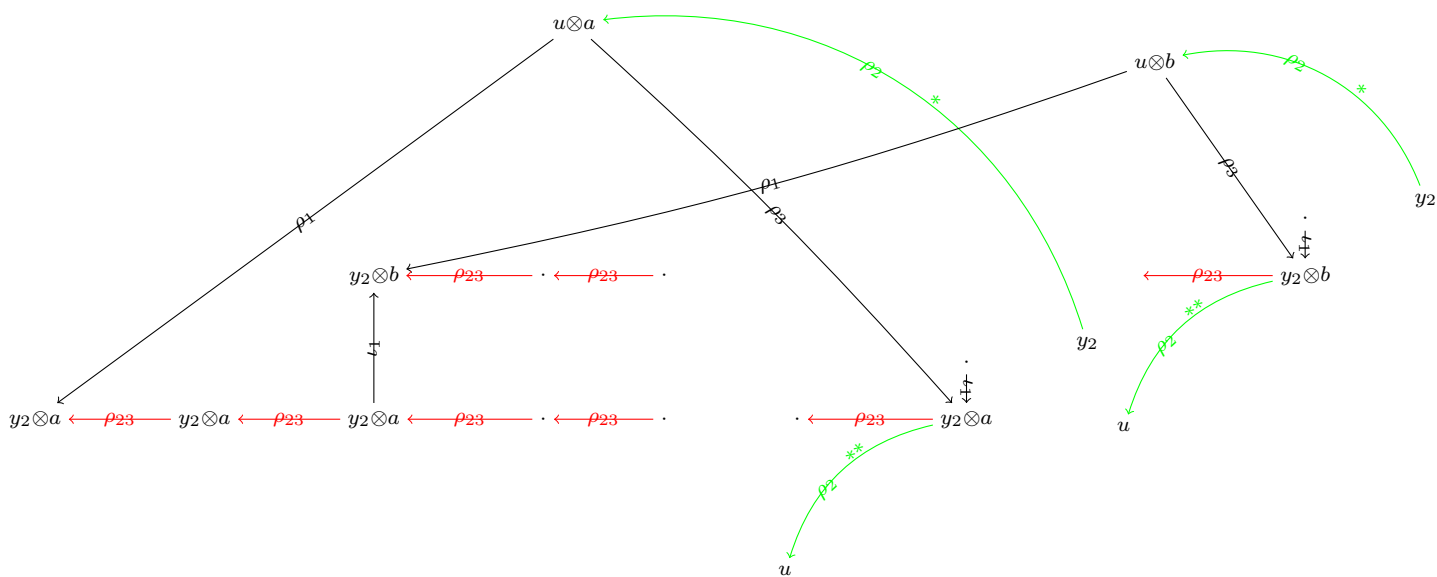
Figure 31: V^0

Figure 32: V^0

Figure 33: V^0



(a)



(b)

Figure 34: V^0

Now we tackle the most complicated case: a $a \rightarrow b$ arrow in ∂_w with length 1, see fig. 35. In this case, a at the left-most position has both the incoming ρ_3 and the outgoing ρ_2 . ρ_{123} also appears as the length of the arrow is 1. We first assume b has no outgoing length 1 ∂_z arrows. So no downward going black arrows from the second b from the right.

Now we take the tensor, with fig. 24b in section 3.4.2 in mind. All potential green arrows marked with $*$ appear again, except b 's y_2 doesn't have one going out as b has no length one ∂_z arrow. The pink ρ_{123} doesn't lead to any new arrows, as argued in section 3.4.2, see fig. 36. Then, cancel the middle two pairs of reds, yielding only the two desired ρ_{23} 's. Then, cancel the two $x_1 \rightarrow v$'s "for free". Then, cancel the two $x_2 \rightarrow y_3$'s "for free", see fig. 37. Next, cancel the pair of reds on the left side, again put u 's on top. Then cancel the two $x_3 \rightarrow y_1$'s. Now see fig. 38. It matches $KtD(C^{flip})$ in a similar fashion as fig. 34.

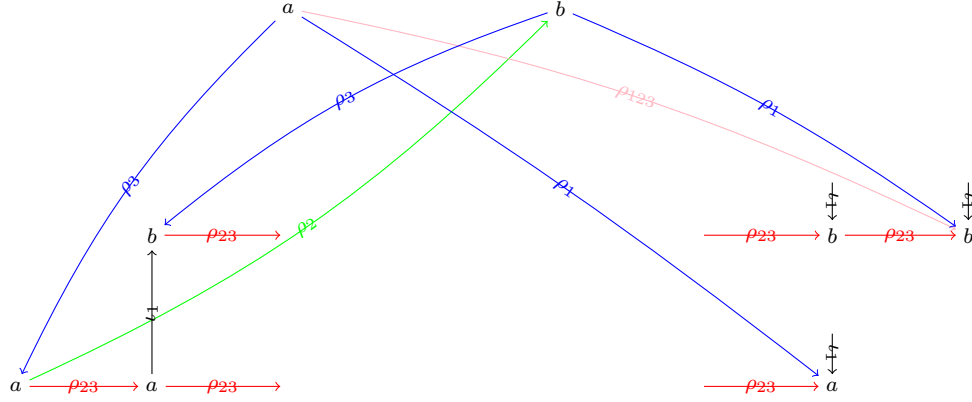
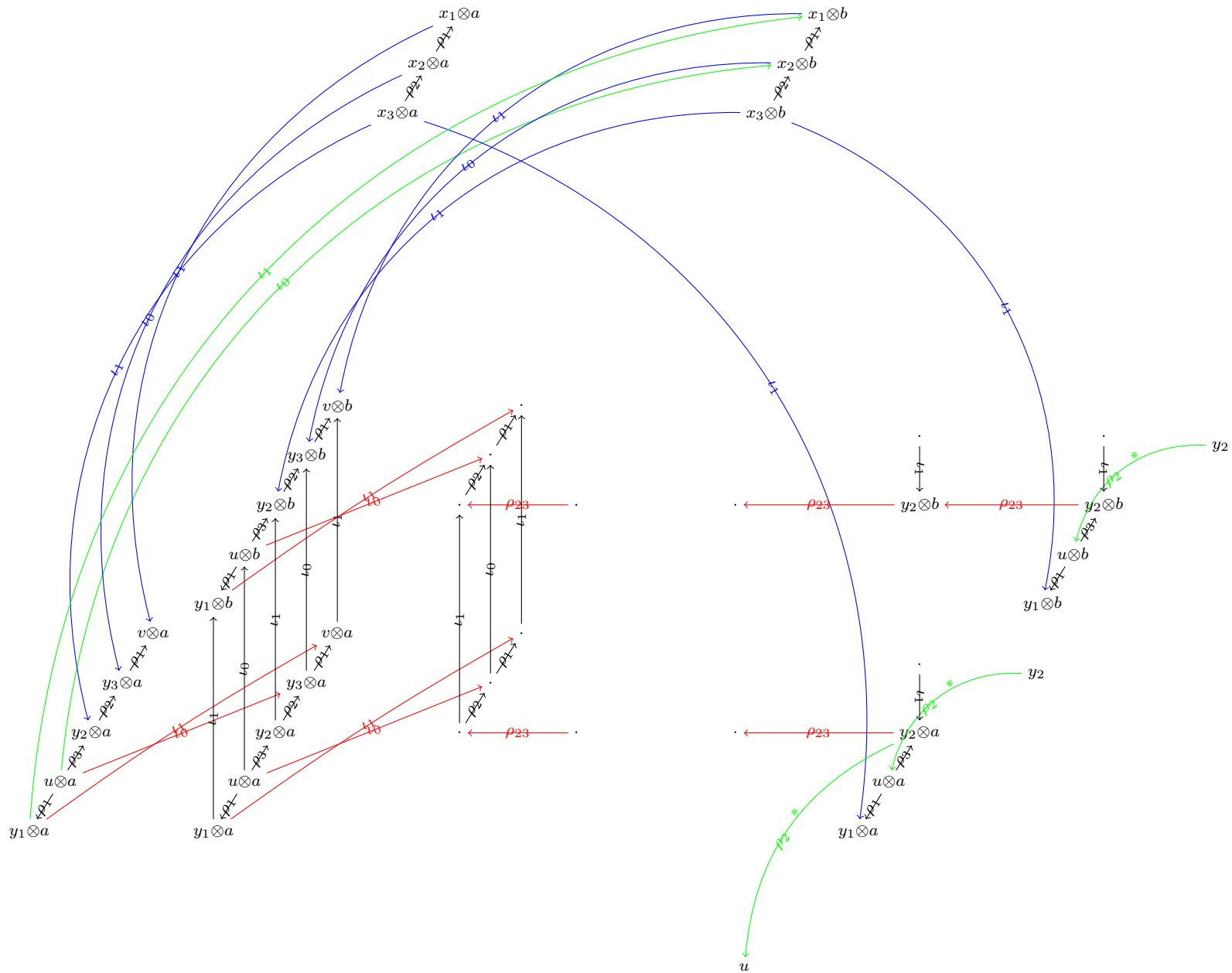
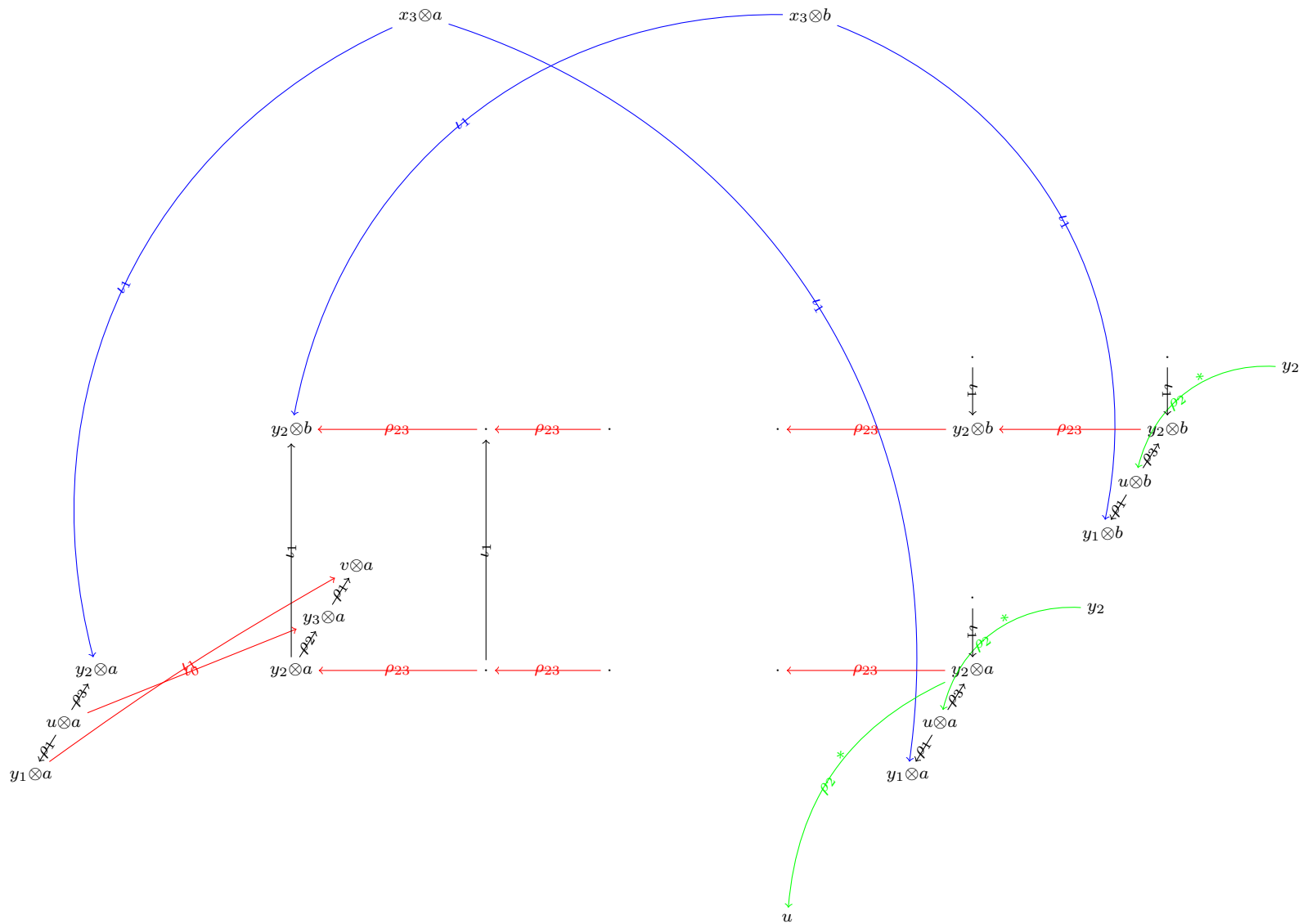


Figure 35: V^0

Figure 36: V^0

Figure 37: V^0

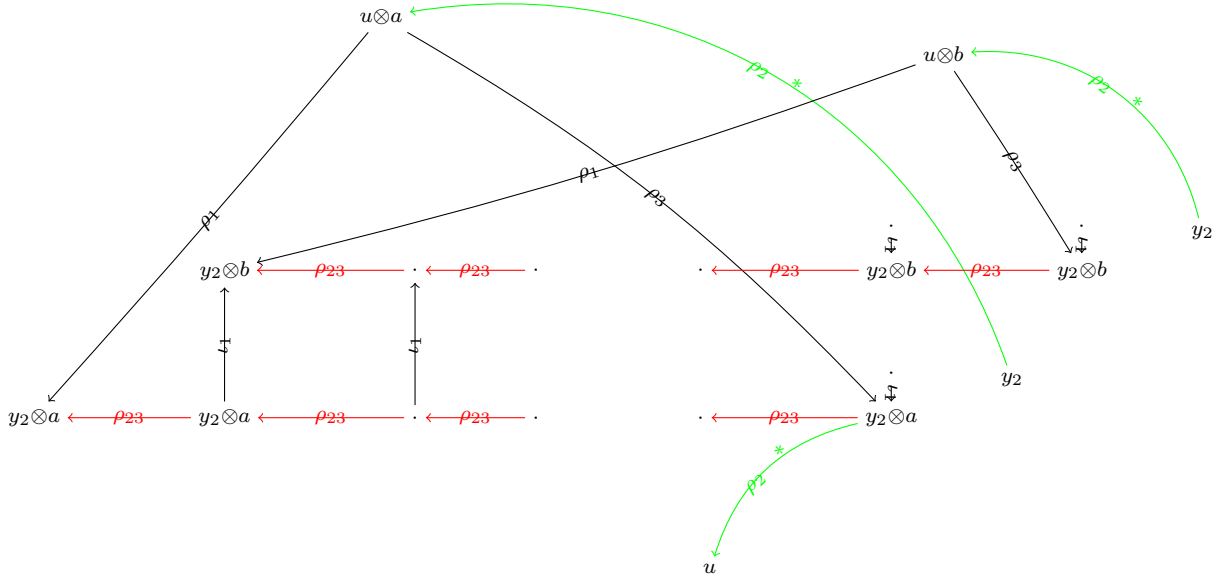


Figure 38: V^0

Now we consider the possibility of an outgoing length 1 arrows $b \rightarrow c$ in ∂_z . (c can not be the same as a , because that $d^2 = 0$ and horizontal simplifiedness would force C to be infinitely generated.) To ensure $d^2 = 0$, there must be a generator d in one Alexander filtration level below a to form this 1 by 1 box in C , as in fig. 39. We do not exclude the possibility of other incoming or outgoing vertical arrows at the generators. fig. 40 shows the corresponding part in $KtD(C)$. fig. 41 shows the tensor product before any cancellation are applied. The open-ended purple arrows are potential arrows. Now we apply the cancellation described in section 3.4.2 on the right side. Then make some “free” cancelations: cancel all blue $x_1 \rightarrow v$ ’s and then all $x_2 \rightarrow y_3$ ’s, which generate no new arrows. Next, we cancel all the pairs of reds on the left-hand side. All those cancelations have been previously described in details, so we just show the final result in fig. 42.

A few things to point out here: Arrows marked with $*$ (eight green and one pink) are those dangling arrows in fig. 24b. They exist because of the potential ∂_z differentials connecting to a, b, c, d (purple ones in fig. 39). The two green arrows marked by $**$ are the same kind of dangling arrow whose two ends we finally see in one diagram, as they come from the arrows $b \rightarrow c$ and $a \rightarrow d$ in ∂_z . The pink arrow marked with $**$ is also a manifestation of of the pink dangling arrow in fig. 24b.

Next, we move y_1 ’s and u ’s to the top, and cancel $x_3 \rightarrow y_1$ at b in V^0 , then that

arrow at a in V^0 , then that arrow at c in V^0 , then that arrow at d in V^0 , see fig. 43. Now everything matches to $KtD(C^{flip})$ as described above, except we are missing two ρ_{123} 's. For convenience, we label the u 's in V^0 with the generator it corresponds: u^a, u^b, u^c, u^d and label the y_2 's on the left hand side with the row it is in and the its distance to the leftmost position: $y_2^{d,0}, y_2^{c,1}$, etc. y_2 's on the right hand side are similarly labeled as $y_2^{d,0,r}, y_2^{c,1,r}$, etc. Per lemma 2, there must be two ρ_{123} 's from u^a to $y_2^{d,0}$ at the left-most position of d 's row on the left, and from u^b to $y_2^{c,0}$. We also have an extra arrow from u^a to $y_2^{c,0}$ (partially pink in the diagram).

To fix this, we do a change of basis: $\langle u^a, u^b, y_2^{d,1}, y_2^{c,1} \rangle \rightarrow \langle u^a + \rho_1 y_2^{d,1}, u^b + \rho_1 y_2^{c,1}, y_2^{d,1}, y_2^{c,1} \rangle$, where d and c are circled and boxed respectively on the diagram. We examine the effect of this change of basis. u^a : $\rho_2 u^a = \rho_2(u^a + \rho_1 y_2^{d,1})$, so its incoming dangling ρ_2 arrow is unaffected. $\partial u^a = \rho_1 y_2^{a,0} + \rho_1 y_2^{c,0} + \rho_3 y_2^{a,0,r}$ and $\partial(u^a + \rho_1 y_2^{d,1}) = \rho_1 y_2^{a,0} + \rho_1 y_2^{c,0} + \rho_3 y_2^{a,0,r} + \rho_1(\rho_{23} y_2^{d,0} + y_2^{c,0}) = \rho_1 y_2^{a,0} + \rho_3 y_2^{a,0,r} + \rho_{123} y_2^{d,0}$, which is exactly what we need. For u^b , its incoming dangling ρ_2 arrow is also unaffected. $\partial u^b = \rho_1 y_2^{b,0} + \rho_3 y_2^{b,0,r}$ and $\partial(u^b + \rho_1 y_2^{c,1}) = \rho_1 y_2^{b,0} + \rho_3 y_2^{b,0,r} + \rho_1 \rho_{23} y_2^{c,0} = \rho_1 y_2^{b,0} + \rho_3 y_2^{b,0,r} + \rho_{123} y_2^{c,0}$, which is also what we need. See fig. 44 for the final product. Note the dangling partially pink arrow will function as the extra arrow $**$ in fig. 43 for some other 1 by 1 box starting at d , should there exist one.

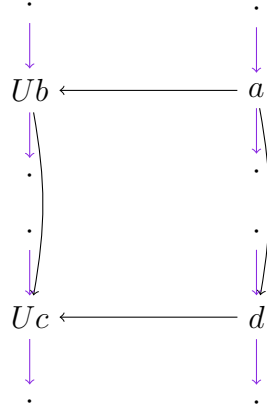


Figure 39: V^0

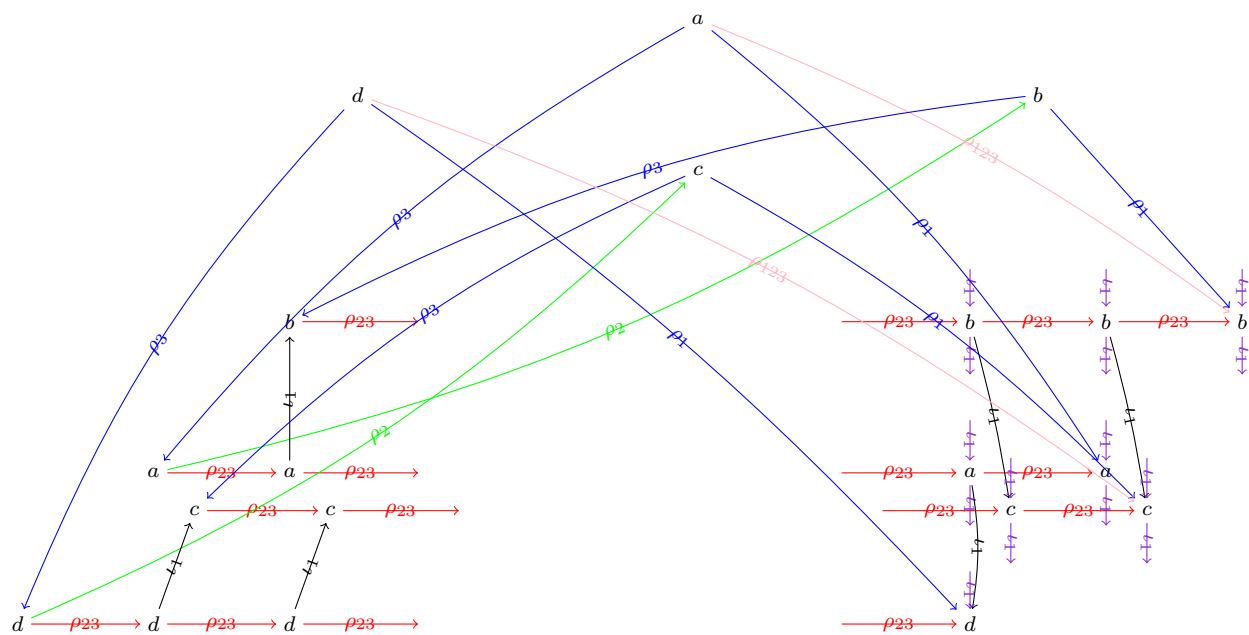
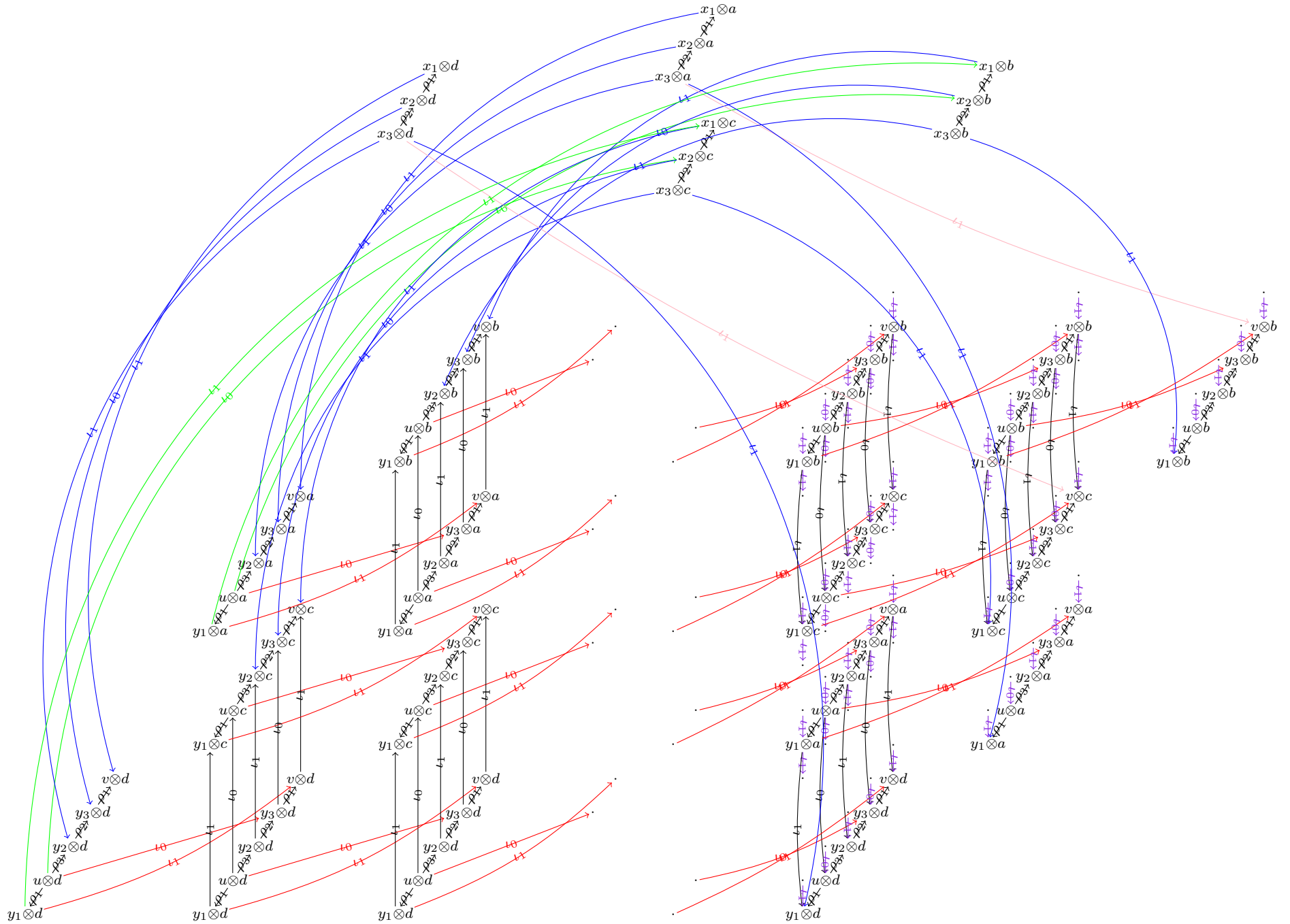
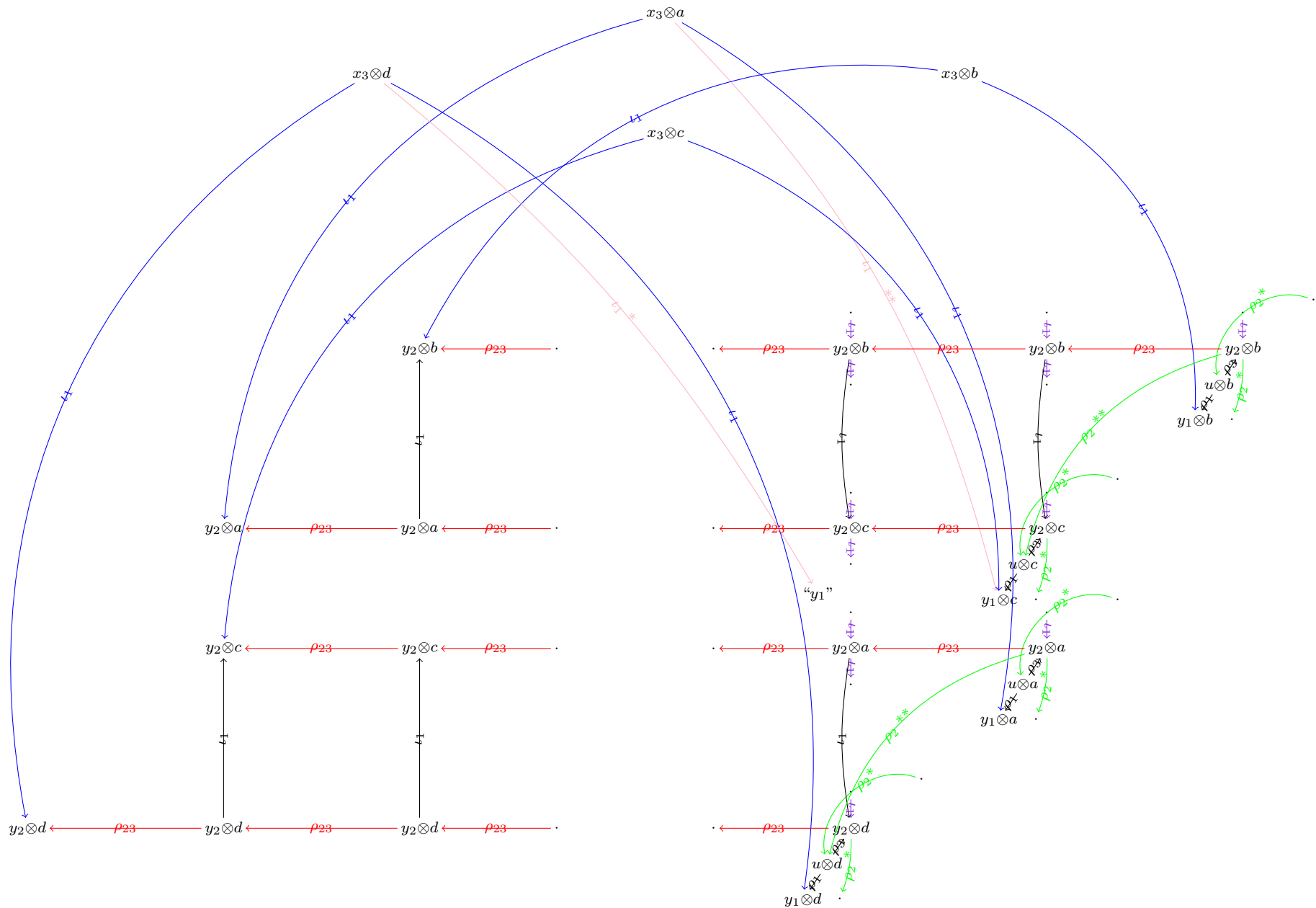
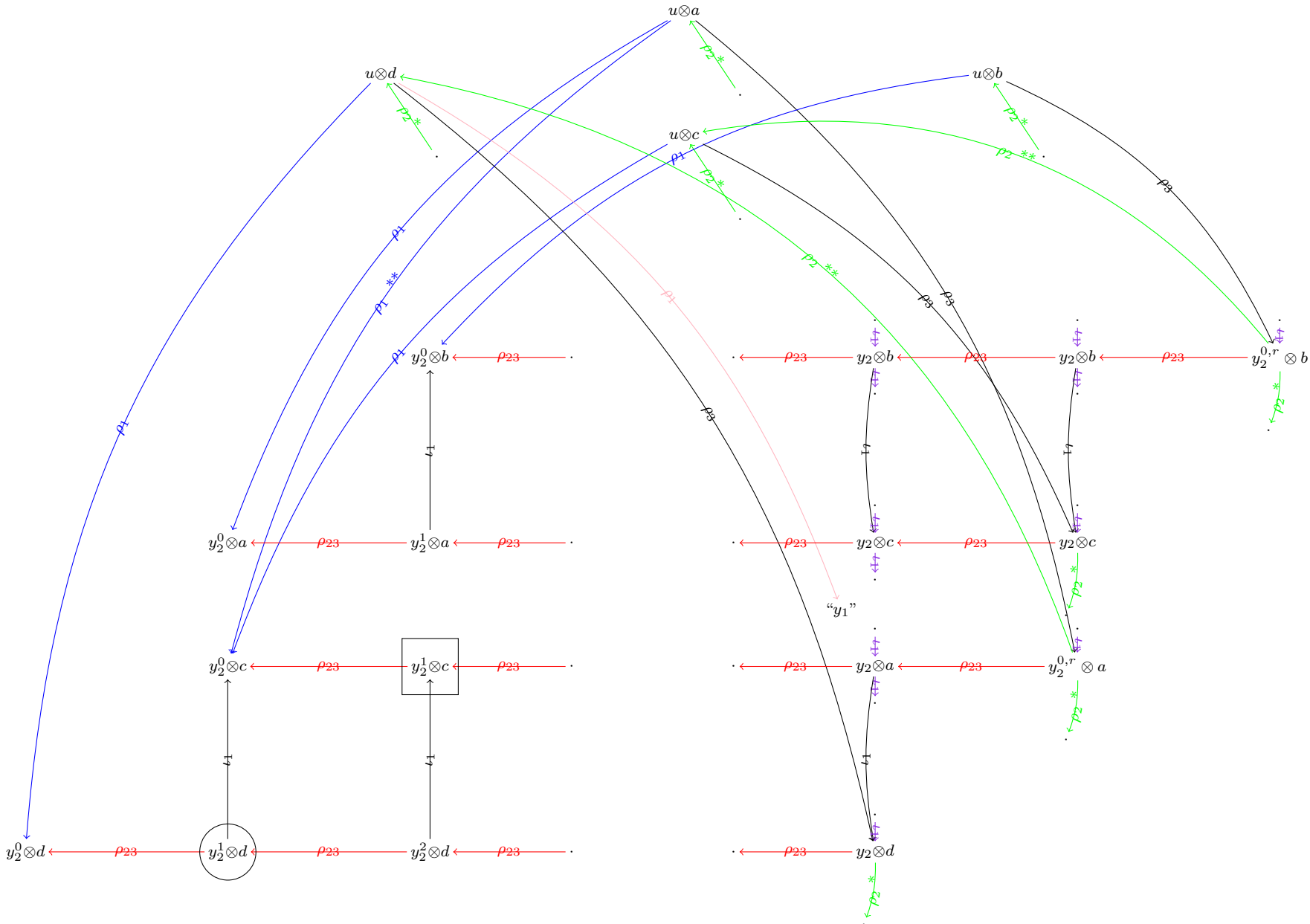
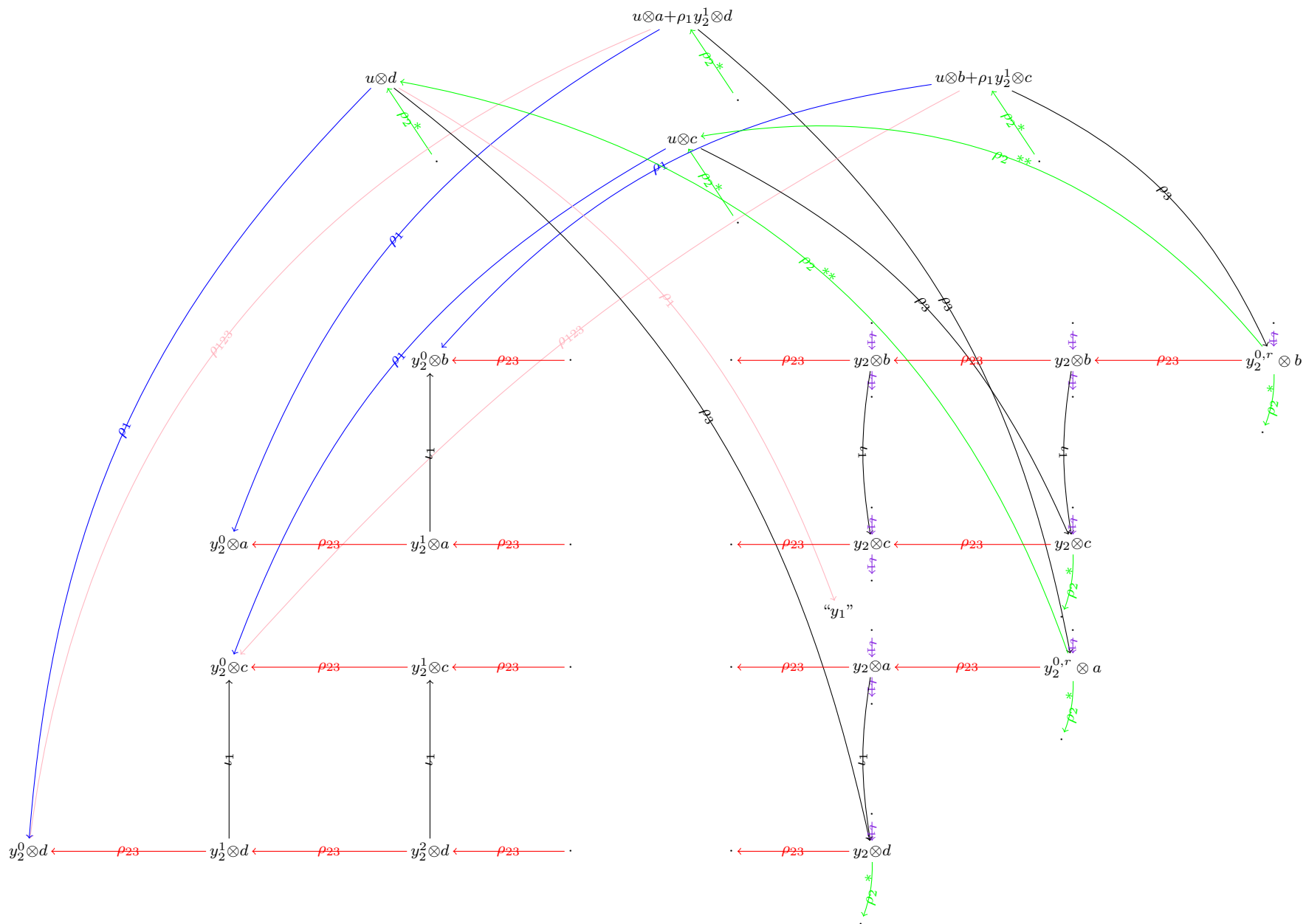


Figure 40: V^0

Figure 41: V^0

Figure 42: V^0

Figure 43: V^0

Figure 44: V^0

3.4.6 Left hand side full copy

The situation at left hand side full copy is simpler than the right hand side, as C is horizontally simplified. Generators come in pairs except ξ_h , which is generator of the homology, see fig. 45a for a pair $x \rightarrow y$ and ξ_h . The isomorphism-inducing map between the full copy and \mathbb{F}_2 must be a single arrow from ξ_h to the generator of \mathbb{F}_2 .

At a pair $x \rightarrow y$, we cancel the pairs of red arrows, which we have done so many times, see fig. 45b. Then we cancel the vertical black arrows between y_1 's and u 's, see fig. 45d. At the row of ξ_h , it is even simpler. It is now a single string of ρ_{23} 's. The usual cancellation bring them into shape.

One last corner case is of the top row, where the full copy meets the left-most position of a row. We need to examine that the cancellation needs to be done in both places are compatible. It is clear that the top row generator has only incoming ρ_3 , but no outgoing ρ_2 . We further observe that the cancellation in section 3.4.5 only concern y_3, v at the top row generator, whereas cancellation in this section remove y_1, u there. This means the two sets of cancellation never interact, hence must be compatible.

3.4.7 Conclusion of proof

Therefore, we have examined all parts of the modules and can conclude that tensoring with H indeed transforms $KtD(C)$ to $KtD(C^{flip})$. Hence Proposition 2 is proved.

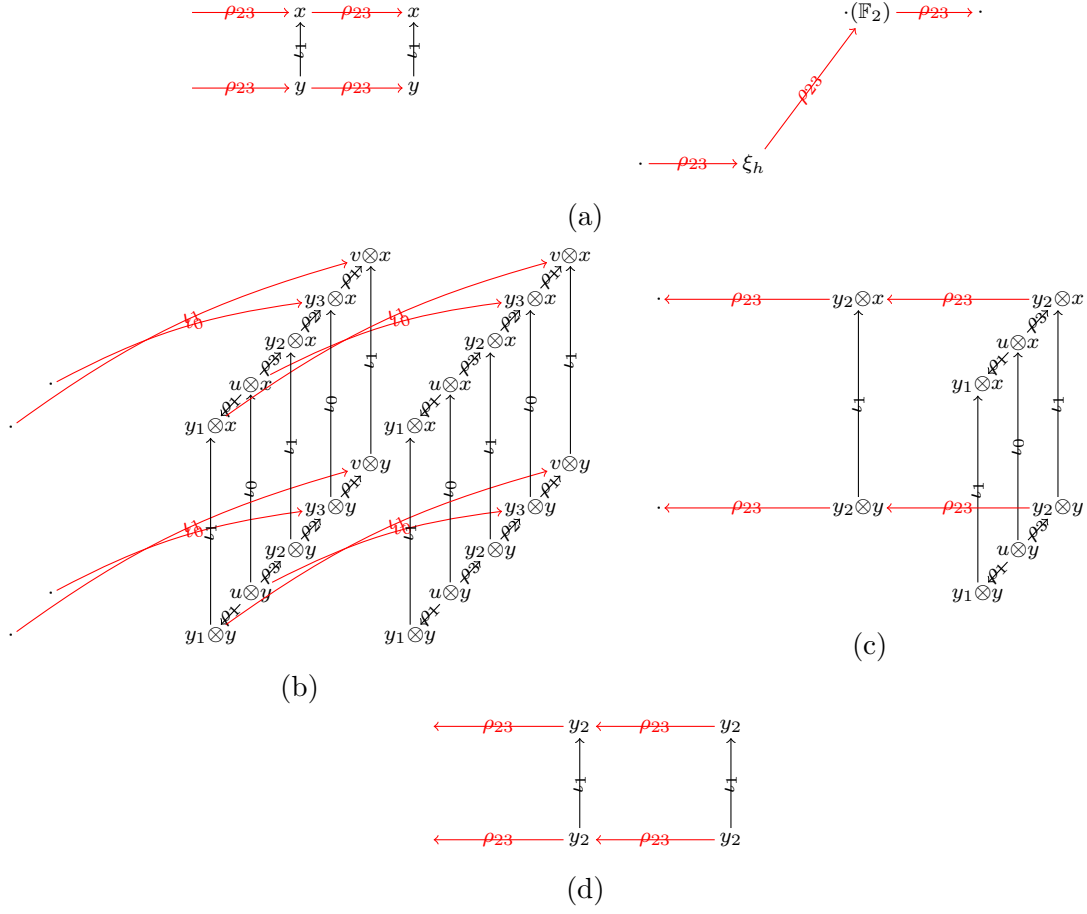


Figure 45: Left hand side full copy

References

- [1] Jacob Rasmussen, *Floer homology and knot complements*, Ph.D. thesis, Harvard University, Cambridge, MA, 2003, arXiv:math.GT/0306378.
- [2] Peter S. Ozsváth and Zoltán Szabó, *Holomorphic disks and topological invariants for closed three-manifolds*, Ann. of Math. (2) 159 (2004), no. 3, 1027-1158, arXiv:math.SG/0101206.
- [3] Benson Farb, Dan Margalit, *A Primer on Mapping Class Groups*. Princeton University Press, 2011.
- [4] Robert Lipshitz, Peter S. Ozsváth, and Dylan P. Thurston, *Bordered Heegaard Floer homology: Invariance and pairing*, 2008, arXiv:0810.0687v5.
- [5] Robert Lipshitz, Peter S. Ozsváth, and Dylan P. Thurston, *Bimodules in bordered Heegaard Floer homology*, 2010, arXiv:1003.0598v3.
- [6] Peter S. Ozsváth and Zoltán Szabó, *Holomorphic disks and knot invariants*, Adv. Math. **186** (2004), no. 1, 58-116, arXiv:math.GT/0209056.
- [7] Corrin Clarkson, *Three-manifold mutations detected by Heegaard Floer homology*, 2013, arXiv:1310.3282v2.